STRENGTHENING OF NiAl MATRIX COMPOSITES

Prepared by
R. J. Arsenault

ANNUAL REPORT
N00014-94-10118

Prepared for

Office of Naval Research
800 North Quincy Street
Arlington, Virginia 22217

November 1995

Metallurgical Materials Laboratory
Department of Materials and Nuclear Engineering
University of Maryland, College Park, Maryland 20742-2115

DISCLAIMER NOTICE

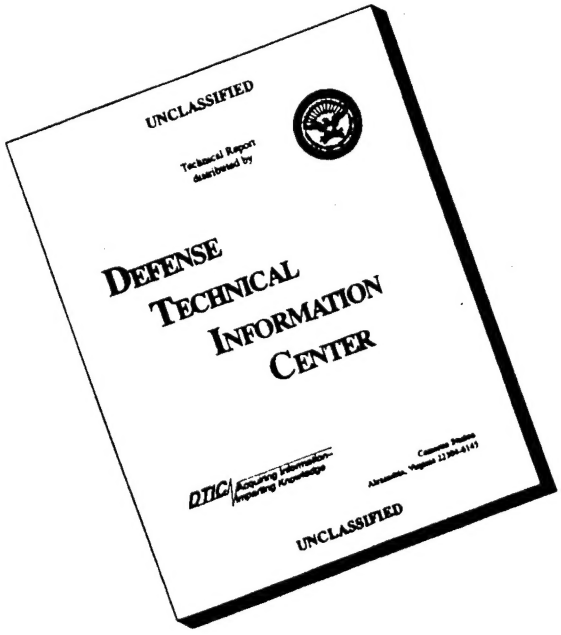

THIS DOCUMENT IS BEST QUALITY AVAILABLE. THE COPY FURNISHED TO DTIC CONTAINED A SIGNIFICANT NUMBER OF PAGES WHICH DO NOT REPRODUCE LEGIBLY.

REPORT DOCUMENTATION PAGE

Form Approved
OMB No 0704 0188

1. AGENCY USE ONLY (Leave blank)	2. REPORT DATE	3. REPORT TYPE AND DATES COVERED
	Nov. 30, 1995	Annual Report, Oct. 1, 1994–Nov. 30, 1995

4. TITLE AND SUBTITLE
Stengthening of NiAl Matirix Composites

5. FUNDING NUMBERS
N00014-94-10118

6. AUTHOR(S)
R.J. Arsenault

7. PERFORMING ORGANIZATION NAME(S) AND ADDRESS(ES)
University of Maryland
College Park, MD 20742-2115

8. PERFORMING ORGANIZATION REPORT NUMBER
MML-1-1994

9. SPONSORING/MONITORING AGENCY NAME(S) AND ADDRESS(ES)
Office of Naval Research
800 North Quincy Street
Arlington, VA 22217

10. SPONSORING/MONITORING AGENCY REPORT NUMBER

11. SUPPLEMENTARY NOTES

12a. DISTRIBUTION/AVAILABILITY STATEMENT
Unlimited

12b. DISTRIBUTION CODE

13. ABSTRACT (Maximum 200 words)

Executive Summary

A detailed mechanism has been developed which will predict the formation of vacancy-producing jogged-screw dislocations. The motion of these screw dislocations is the thermally-activated rate-controlling mechanism for both the matrix and the NiAl matrix composites. With the exception of very small subgrain or grain sizes and Al_2O_3 particle size (0.5 μm), the internal stress is independent of stress and temperature. The increase in the internal stress caused by the reinforcement is the strengthening mechanism.

The apparent unusual result of an increase in dislocation density due to relaxation of the thermal residual stress as the particle size increases in Al_2O_3/NiAl composites has been explained by a new model. This model, which employs FEM and crystal plasticity, is based on the low symmetry of the NiAl B2 crystal structure which results in a paucity of independent slip systems.

14. SUBJECT TERMS	15. NUMBER OF PAGES
Discontinuous Intermetallic Matix Composites, Al_2O_3/NiAl, Internal Stress Strengthening, Jogged Screw Dislocation	48
	16. PRICE CODE N/A

17. SECURITY CLASSIFICATION OF REPORT	18. SECURITY CLASSIFICATION OF THIS PAGE	19. SECURITY CLASSIFICATION OF ABSTRACT	20. LIMITATION OF ABSTRACT
Unclassified	Unclassified	Unclassified	N/A

Executive Summary

A detailed mechanism has been developed which will predict the formation of vacancy-producing jogged-screw dislocations. The motion of these screw dislocations is the thermally-activated rate-controlling mechanism for both the matrix and the NiAl matrix composites. With the exception of very small subgrain or grain sizes and Al_2O_3 particle size (0.5 μm), the internal stress is independent of stress and temperature. The increase in the internal stress caused by the reinforcement is the strengthening mechanism.

The apparent unusual result of an increase in dislocation density due to relaxation of the thermal residual stress as the particle size increases in Al_2O_3/NiAl composites has been explained by a new model. This model, which employs FEM and crystal plasticity, is based on the low symmetry of the NiAl B2 crystal structure which results in a paucity of independent slip systems.

TABLE OF CONTENTS

I. Introduction

A detailed mechanism has been developed that will predict the formation of Vacancy-Producing (VP) jogged screw dislocations. Based on a review of the mechanism of non-conservative motion of jogged screw dislocations for steady state creep it was concluded that only the motion of screw dislocations that contain VP jogs is capable of predicting the correct relationship between stress and strain rate in a creep test. Strain rate vs applied stress for the VP jogged screw dislocation model was formulated. Long screw dislocations with jogs or super jogs were observed in NiAl matrix composites after plastic deformation. It has been postulated that the mechanical behavior of NiAl matrix composites can be based on the mechanism of thermally-activated motion of these jogged screw dislocations. By computer simulation, it was found that the VP jog model can predict with good accuracy the yield stress and temperature dependence of NiAl composites.

A simple model based on the cross-slip of screw dislocations in NiAl is proposed to account for the VP jogs. In this model, kinks change into a single type of jog after a screw dislocation cross slips. Figures 1a-d and 2 show schmetically how this mechanism works. The change from kinks into jogs is a simple process because of the crystal geometry of the B2- ordered

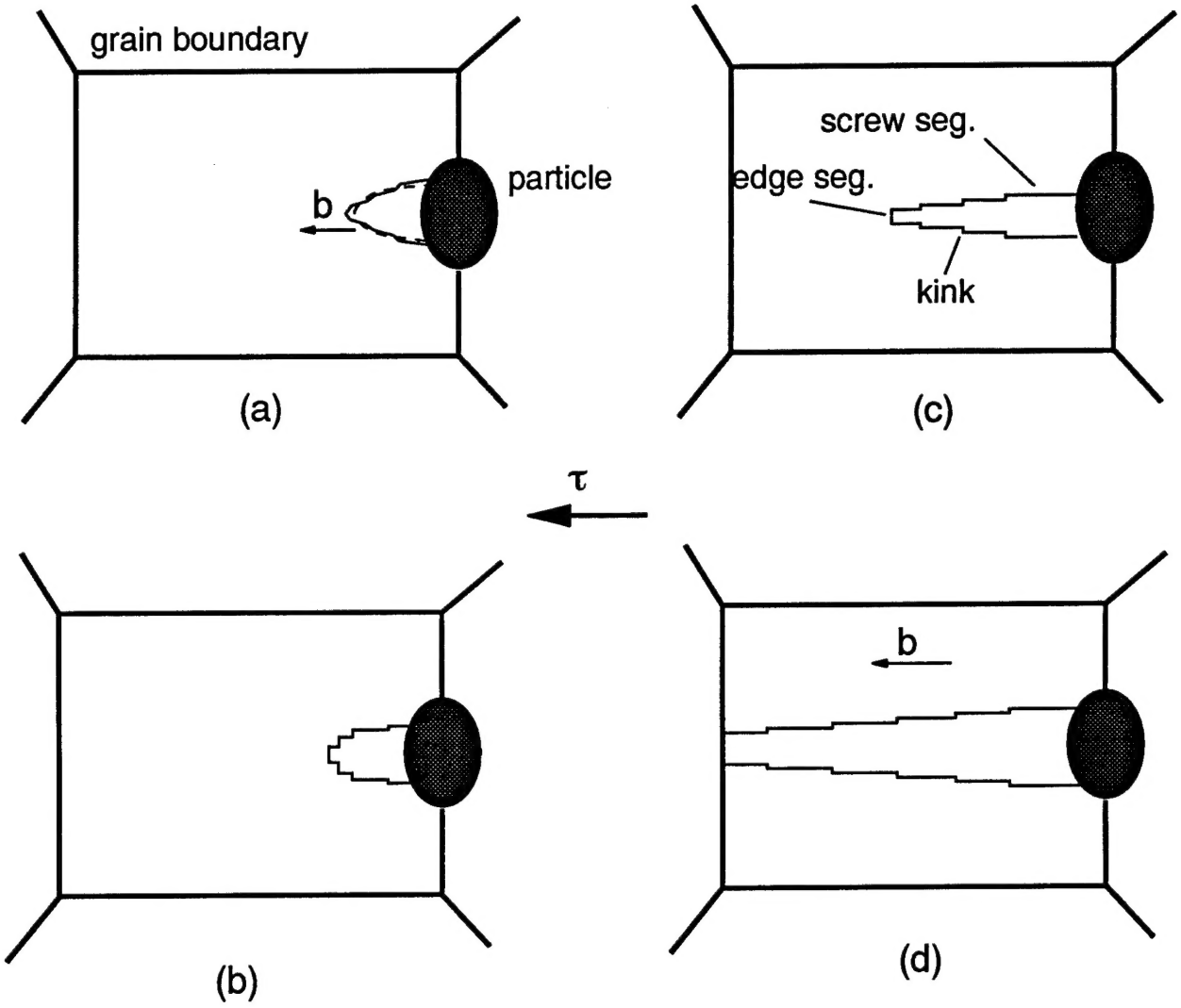

Fig 1. (a) Zig-zag dislocation is generated from the interface of particle and matrix. (b) Zig-zag dislocation is stretched by applied stress. (c) Dislocation is bowing out upon applied stress. (d) Final dislocation configuration.

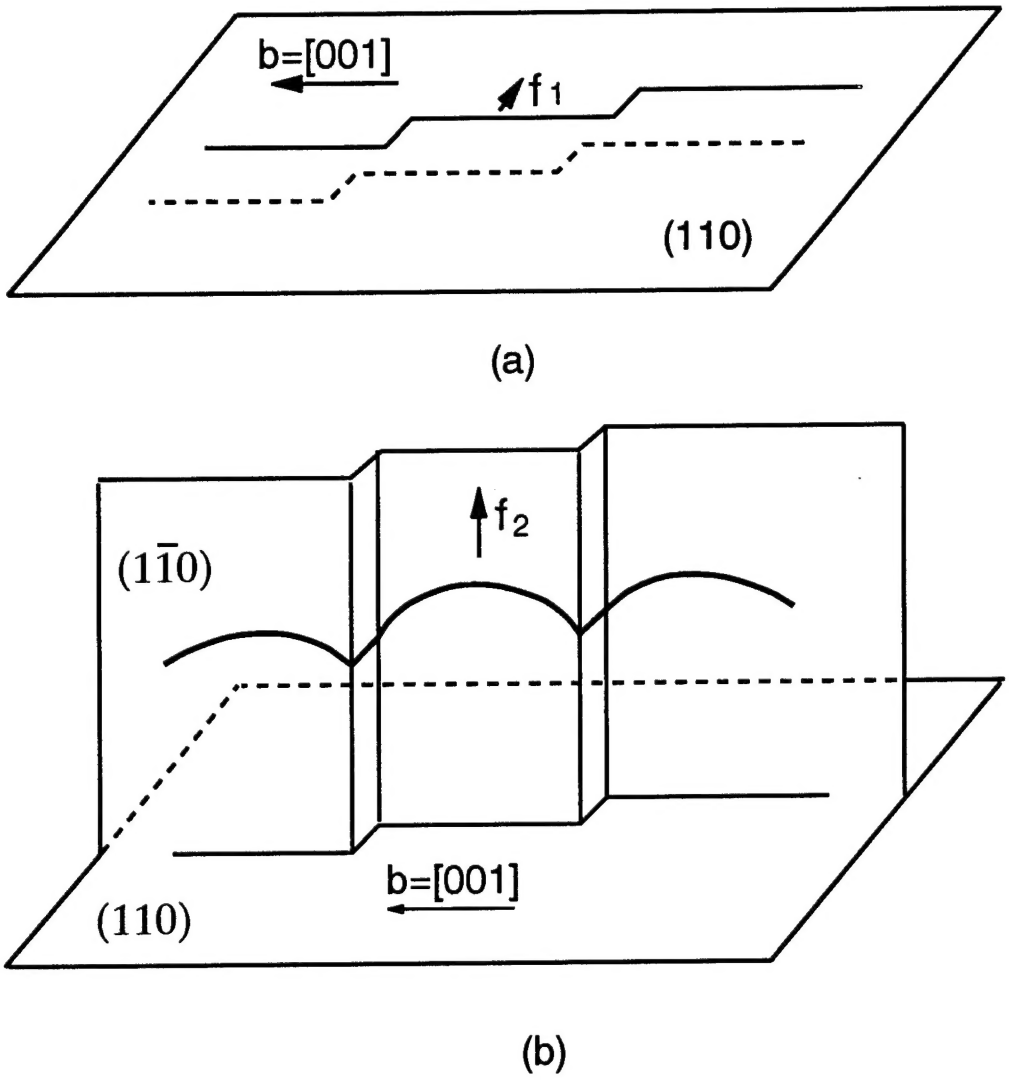

Fig 2. A screw dislocation before (a) and after (b) cross slip.
(a) f_1 drives the screw dislocation move on (110).
(b) when f_1 is overcomed by obstacles, the screw dislocation tries to move on the second slip plane ($1\bar{1}0$) under f_2, the same sign jogs sign are produced.

structure. This model may provide the necessary conditions for a mechanism of jogged screw dislocation, as well as an explanation of why jogs prefer to move by producing vacancies.

It was recently shown that when the particle size is further reduced from 5μm to 0.5μm, there is an increase in strength at low temperatures (room temperature) but, at high temperatures (1000°C) the composite is weaker than the matrix material and also the 5μm composite (as shown in Fig. 3). This result contradicts the previous results, which showed that a decrease in Al_2O_3 and matrix subgrain or grain size results in strengthening at all temperatures. This recent result is probably an indication that the thermal strengthening produced by 0.5μm Al_2O_3 and 0.5μm NiAl particle size is <u>not</u> independent of stress and temperature.

An area which has been difficult to understand is the "apparent" lack of generation of dislocations in the NiAl matrix due to relaxation of the thermal residual stress (TRS). A more extensive investigation was undertaken to determine the effect of size and shape of Al_2O_3 on the relaxation of the TRS. The dislocation density and thermal residual elastic strain were measured in NiAl matrices of 20 (V%) Al_2O_3 discontinuously-reinforced composites. As the size of the reinforcement

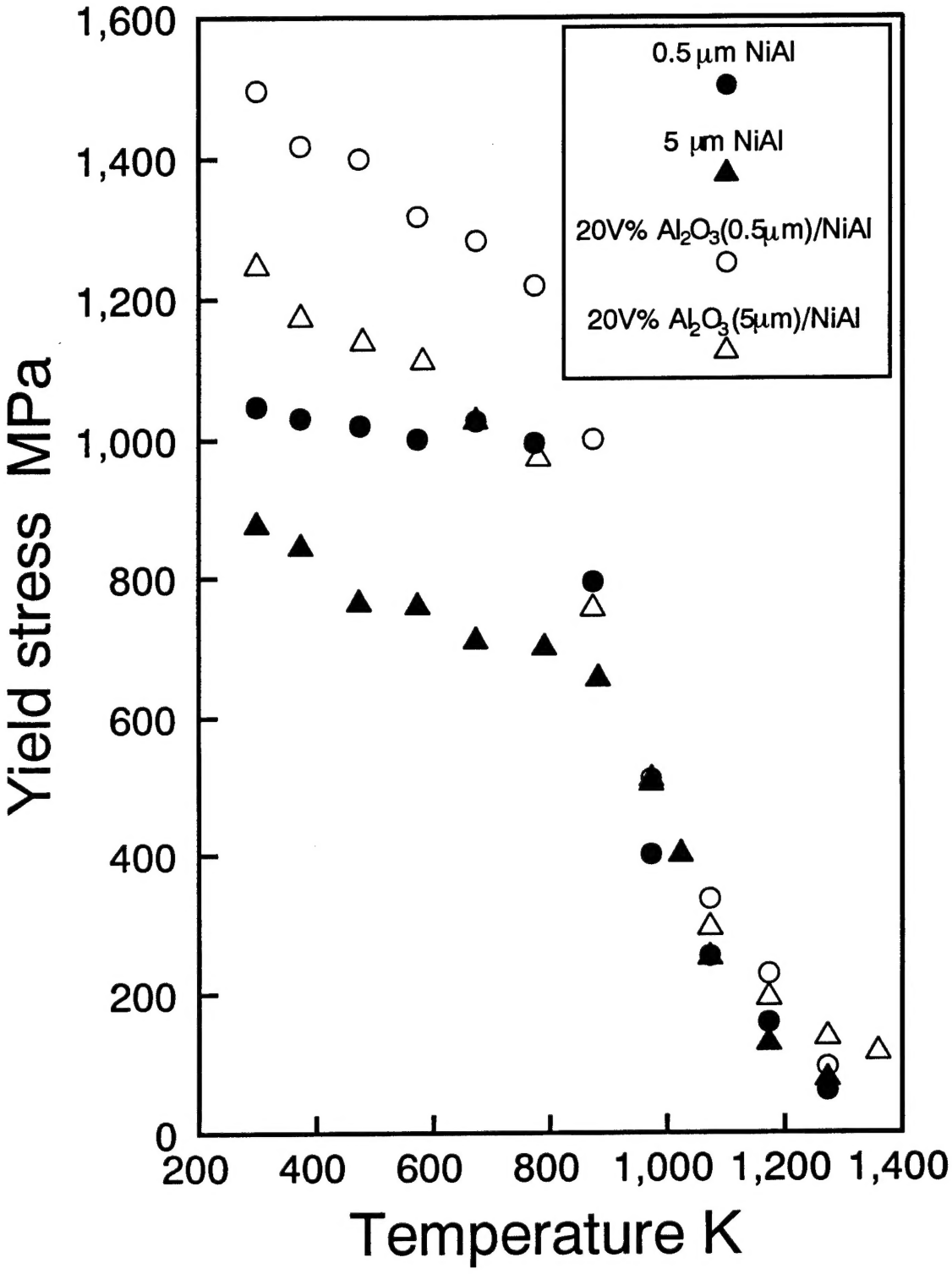

Fig 3. Yield stress vs Temperature of NiAl composites

increased the average dislocation density increases, and the corresponding thermal residual elastic strains decreased. The changes with respect to particle size in the dislocation density and residual strain can neither be explained by continuum theories nor by dislocation mechanics for a homogeneous medium. A previously developed model (that satisfactorily describes the SiC/Al system) suggests that the misfit dislocation density decreases with an increase in reinforcement size but this disagrees with the current Al_2O_3/NiA results. A new model, which employs FEM and crystal plasticity, was proposed to describe how low-symmetry intermetallics, are constrained in their ability to relax the thermal mismatch because of a paucity of independent slip systems.

There are still some remaining investigations which are being completed on SiC/Al composites. SiC/Al composites have interesting mechanical properties (e.g., the tensile yield stress is less than the compressive yield stress; whereas, the apparent modulus in tension is greater than that in compression). The Bauschinger effect of SiC/Al composites is also asymmetric with regard to loading directions. Quantitative measurements of the asymmetry of the composite Bauschinger effect were made and the origin of this asymmetrical Bauschinger effect was investigated. We have successfully reconstructed the observed asymmetry using

an internal stress model based on the development of an internal stresses, conveniently referred to as the "back stress", and work hardening.

The following are: a list of publications, a list of presentations and a selected few publications:

II. List of Publications
(papers published and submitted, book chapters and invited reviews)

1. INTERFACES IN CONTINUOUS FILAMENT REINFORCED Al_2O_3/NiAl COMPOSITES
   L. Wang, K. Xu, R.R. Bowman and R.J. Arsenault
   Met. Trans. 26A, 1995, 897.

2. ANOMALOUS PENETRATION OF AL INTO SIC
   J.C. Romero and R.J. Arsenault
   Acta Met. 43, 1995, 849-857.

3. A Comparison of Interfacial Arrangements of SiC/Al Composites
   R.J. Arsenault and J. Romero
   Scripta Mat.,32, 1995, 1783-1787.

4. INTERFACIAL STRUCTURE OF A SIC/AL COMPOSITE
   J.C. Romero and R.J. Arsenault
   Accepted for publication in Mat. Sci. & Eng.

5. Effect of Particle Type and Shape on the Strengthening of NiAl Matrix Composite
   J. Liu, K. Xu and R. J. Arsenault
   ICCM 10, ed. by K. Street and A. Poursantip, 1995, Vol.II, pp. 785-792.

6. Relaxation of Thermal Mismatch in Discontinuously Reinforced Composites
   N. Shi, R. J. Arsenault, M. A. M. Bourke and J. A. Goldstone
   J. C. M. Li Seventieth Birthday Symposium, Ed. By S.N.G. Chu, P.K. Liaw, R. J. Arsenault, K. Sadananda, K. S. Chan, W. W. Gerberich, C. C. Chau and T. M. Kung, TMS, 1995, p. 435.

7. Interface in Intermetallic Matrix Composites
K. Xu, L. Wang and R.J. Arsenault
High Performance Composites, Ed. by K.K. Chawla and P. Laiw, TMS, 1994.

8. Composite Ductility - The Role of Reinforcement and Matrix
N. Shi and R.J. Arsenault
Intrinsic and Extrinsic Fracture Mechanisms in Discontinuously Reinforced Composites, Ed. by J.J. Lewandowski and W.H. Hunt Jr., TMS 1995.

9. Stress Relaxation in Discontinuously Reinforced Composites
N. Shi and R. J. Arsenault
Symposium on Micro mechanisms and Constitutive Modeling of Composites, Ed. by I. Demir and H. Zbib, AMD vol. 202/ MD vol.61, 1995, p. 39.

10. Discontinuously Reinforced Composites
Advanced Composites Newsletter, Ed. by Y.R. Mahajan
vol. 4, No. 2, 1995, p.6.

11. Bauschinger Effect in A SiC/Al Composite N. Shi, U.T.S. Pillai and R. J. Arsenault J.M.C. Li Seventieth Birthday Symposium, Ed. by S.N.G. Chu, P.K. Liaw, R. J. Arsenault, K. Sadawanda, K. S. Chan, W. W. Gerberich, C.C. Chau and T. M. Kung, TMS, 1995, p. 435.

12. Deformation and Fracture Behavior of Metal-Ceramic Matrix Composite Materials
R. J. Arsenault, S. Fishman and M. Taya
Ed. By J. Christian and T. Massalski
Progress in Materials Science, Vol. 38, 1994, pp. 1-157.

13. DISLOCATION IN CONTINUOUS FILAMENT REINFORCED W/NiAl and Al_2O_3/NiAl COMPOSITES
L. Wang, R.R. Bowman and R.J. Arsenault
Submitted for publication.

14. MICROSTRUCTURAL CHANGES DURING CREEP OF A SIC/AL_2O_3 COMPOSITE
J.C. Romero R. Krause and R.J. Arsenault
Mat. Sci. And Eng. A201, 1995, 13-23.

III. List of Presentation

1. Los Alamos National Laboratory, Feb., 1995 "A Review of Strengthening and Asymmetrical Behavior of DMMC".

2. Symposium on Micromechanics and Constitutive Modeling of Composite Materials 1995, "Stress Relaxation in Discontinuously Reinforced Composites"
N.Shi and R. J. Arsenault.

3. Symposium Dedicated James C.M. Li Seventieth Birthday on Micromechanics of Advanced Materials, Fall 1995, "The Bauschinger Effect in a SiC/Al Composite"
N. Shi, U.T.S. Pillai and R.J. Arsenault.

4. University of Tennessee, Fall 1995, "Interfaces in Metal and Intermetallic Matirx Composites".

5. ASM Chapter, Oak Ridge Tennessee, Fall 1995, "Strengthening of NiAl Matrix Composites".

6. Oak Ridge National Laboratory, Fall 1995, "Interfaces in Metal and Intermetallic Matrix Composites"

7. 17th Annual Metal Matrix Composites Working Group Meeting, "Strengthening of NiAl Matrix Composites".

8. ICCM 10, 1995, "Effect of Particle Type and Shape on the strengthening of NiAl Matrix Composite", J. Liu, K. Xu and R.J. Arsenault.

9. Symposium Dedicated James C.M. Li Seventieth Birthday on Micro Mechanics of Advance Materials, Fall 1995, "Relaxation of Thermal Mismatch in Discontinuously Reinforced Composites", N. Shi, R.J. Arsenault, M.A.M. Bourke and J.A. Goldstone.

IV. Publications (A selected few)

1. ANOMALOUS PENETRATION OF AL INTO SIC
J.C. Romero and R.J. Arsenault
Acta Met. 43, 1995, 849-857.

2. A Comparison of Interfacial Arrangements of SiC/Al Composites
R.J. Arsenault and J. Romero

Scripta Mat.,32, 1995, 1783-1787.

3. INTERFACES IN CONTINUOUS FILAMENT REINFORCED Al_2O_3/NiAl COMPOSITES
L. Wang, K. Xu, R.R. Bowman and R.J. Arsenault
Met. Trans. 26A, 1995, 897.

4. MICROSTRUCTURAL CHANGES DURING CREEP OF A SIC/AL_2O_3 COMPOSITE
J.C. Romero R. Krause and R.J. Arsenault
Mat. Sci. And Eng. A201, 1995, 13-23.

5. Relaxation of Thermal Mismatch in Discontinuously Reinforced Composites
N. Shi, R. J. Arsenault, M. A. M. Bourke and J. A. Goldstone J. C. M. Li Seventieth Birthday Symposium, Ed. By S.N.G. Chu, P.K. Liaw, R. J. Arsenault, K. Sadananda, K. S. Chan, W. W. Gerberich, C. C. Chau and T. M. Kung, TMS, 1995, p. 435.

Pergamon

0956-7151(94)00250-9

Acta metall. mater. Vol. 43, No. 2, pp. 849–857, 1995

0956-7151/95 $9.50 + 0.00

ANOMALOUS PENETRATION OF Al INTO SiC

J. C. ROMERO and R. J. ARSENAULT

Metallurgical Materials Laboratory, Materials and Nuclear Engineering Department,
University of Maryland, College Park, MD 20742-2115, U.S.A.

(Received 20 July 1993; received for publication 27 June 1994)

Abstract—The chemical composition of a SiC/Al interface was investigated after two different annealing conditions. The composite was produced by powder metallurgy methods and it showed remarkable interfacial stability in the as-prepared condition; similar results were obtained as long as the annealing temperature was kept below 650°C. On the other hand, substantial interpenetration was seen when the Al matrix was present in the liquid state. At temperatures above 700°C, the interface was seen to react quite rapidly and to be covered with a thick layer of Al_4C_3; while, at 680°C, the interface acquired a serrated profile along the basal planes of the SiC and substantial amounts of Al were seen to penetrate into the SiC along channels formed due to the break up of the SiC. In such cases, no Al_4C_3 was seen to precipitate in the matrix; instead, $MgAl_2O_4$ and Al_2O_3 were observed but at distances up to 100 nm away from the interface.

INTRODUCTION

The interest metal matrix composites have generated in the past is due to a number of unique properties or possible uses that these new materials possess or are capable of. A case in point is the SiC/Al composite. Composites can be used as structural elements in the automobile and aerospace industry and also in some demanding environments such as the first wall of a fusion reactor. This is due to an improvement in the elastic modulus, yield strength and tensile strength of the composite as compared with the matrix; as well as an improvement in the wear resistance, in the coefficient of thermal expansion and a stronger resistance to stress corrosion cracking [1, 2]. The major drawback, of course, has been a remarkable drop in the ductility and in the toughness of the composite.

The increased strengthening observed is due to the strength of the bond at the interface between the matrix and the reinforcement. A bond of some kind is then required in order for a thermal residual stress (TRS) to develop; the relaxation of such a stress by subsequent dislocation generation and motion, which work hardens the matrix, will then lead to the observed strengthening of the composite [3–5]. A sufficient bond is possible only when good wetting of the reinforcement by the matrix is obtained, and this is very much dependent on the surface properties of the ceramic and the matrix. These properties are the major variables in the success of different fabrication methods to produced composites with the particular interface strengths which will also lead to the best combination of yield strength, fracture toughness and ductility. Processing methods, such as powder metallurgy and liquid infiltration, are techniques wherein the fabrication temperature is such that the ceramic reinforcement is usually in contact with a liquid matrix. The presence of a liquid matrix will have an effect, not only on the ability of the matrix to more readily wet the reinforcement, but also on the chemical stability of the interface [6].

In the past, four different models have been proposed to explain the type of bonding that exists at the interface between Al and SiC; these are: (1) the presence of a SiO_2 film at the interface to which both, the matrix and the reinforcement, adhere to; (2) direct electronic bonding among the atoms across the interface; (3) a chemical bond due to a reaction at the interface that forms another compound, such as Al_4C_3; and (4) diffusion bonding; although the best available data shows very little diffusion even at temperatures close to 2000°C [7–10].

This last model was not expected, but was proposed as an explanation to some experimental results obtained by Arsenault and Pande [11]. Previous experimental evidence for/or against the diffusion of Al into SiC is not conclusive. One fact which seems to be fairly well established has to do with the size (probably the perfection) of the SiC particle. If a freshly cleaned surface on a large particle (i.e. $>250\,\mu$m) is coated or bonded to Al, no interdiffusion at the interface has been found even at temperatures as high as 800°C [9, 10].

Therefore, consideration was given only to any possible diffusion or penetration of Al into particles of SiC smaller than 250 μm which have been produced by ball milling. We now present the results of our investigation which indicate that Al does penetrate into SiC due to the dissolution of SiC when in contact with a liquid Al matrix.

EXPERIMENTAL PROCEDURE

The "diffusion couples" were prepared from powder metallurgy made SiC-20 vol.% particulate/Al composites. Aluminum is known to form a number of other intermetallic compounds at the temperatures that are used in the fabrication of these composites [12, 13]. In order to diminish the possibility of any precipitates segregating at the interface, it was decided to use an 1100 aluminum powder as the matrix with particles of SiC as the reinforcement (the vast majority had the hexagonal alpha structure, although some had the cubic beta structure). To prepare the TEM samples, slices were then cut from these samples, about 0.5 mm in thickness, and a diamond core drill was then used to cut disks, 3.0 mm in diameter. The disks were then ground to about 0.2 mm in thickness and were then dimpled with a 30 μm diamond paste until the thickness at the center of the sample was about 50 μm. The samples were then ion milled in a TECHNICS IV ion mill set at 4 kV and using Ar^+ ions at 20° from the sample. This was done until perforation of the sample was achieved, at which point the angle was decreased to 10° and the ion milling operation was continued for another 30 min in order to obtain a much wider thinner area on the sample; this will make the samples more suitable for TEM investigations since it will increase the area available for X-ray analysis.

Some of the samples were prepared from the "as made" condition, so that no extra annealing treatments were given to these samples. Two different annealing treatments were chosen for the other samples. One set was annealed at 590°C for 500 and 1000 h in order to check the effect that annealing under more stable thermodynamic conditions will have on the interface stability. The other samples were annealed at 680°C, for 3, 7, 15, 30, 120 and 600 min each, to check the effect that contact with a liquid matrix will have on the interface stability. From this final set, some of the samples were then additionally annealed at 590°C for 500 h. Note that the composites were prepared by compaction at 650°C for 2 h, thus, this can also be considered as one additional annealing treatment. Once the compaction was completed, the composite was furnace cooled under load.

Due to the sharp concentration gradients expected at the interface, it is necessary to carefully obtain precise experimental data in order to resolve the discrepancies that have been obtained in the past. This is so because the small distances that are dealt with can give rise to experimental artifacts that will lead to erroneous conclusions concerning the interface composition. For example, these artifacts can come about due to: (1) lack of a sharp and clean interface; (2) beam or sample shift; (3) redeposition of Al onto SiC during ion milling; and (4) fluorescence of Al by Si X-rays.

In order to map concentration gradients present at the interface, use was made of a JEOL 2000 FX-II STEM microscope. A 10 nm beam was employed, at 200 kV, to scan across an interface which was aligned parallel to the electron beam in a thin region of the sample. A high voltage (200 kV), a small beam diameter (10 nm), and thin sections of the sample (<75 nm) were chosen in order to minimize the spatial broadening and spurious fluorescence effects, while still (through the use of a LaB_6 gun) being able to obtain sufficient signals from as small a volume as possible. Any beam or sample shift can be checked by interrupting the EDS counting at previously chosen intervals and comparing the present image and beam positions with those obtained at the original conditions.

A sharp and clean interface, with no Al film lying either on top or bottom of the SiC along the interface, can be checked by the use of a double tilt holder. This film can be the residual effect of either interrupting the ion milling operation before all the Al has been removed or due to the redeposition of Al onto the SiC during the ion milling operation itself. The sample is then tilted sufficiently in both directions and the interface is checked, visually, to see how the SiC image changes with respect to the matrix; if a film is observed on the surface, the particle is disregarded. It must be mentioned that a preliminary study showed how some of the particles contained up to about 20% Al all across the SiC particle; this was most probably due to the redeposition effect during the ion mill operation. It was for this reason that the present samples were then slightly etched with Keller's etch before any X-ray analysis was carried out, by dipping a cotton swab in the solution and placing a small drop on the sample, which was then quickly washed with methanol. Such a procedure removed the extra Al adhering to the SiC surface so that the new counts showed the Al concentration to drop to a value of about 2% its matrix value all across the SiC.

RESULTS

The first step was to obtain a set of concentration gradients across a number of different interfaces in the "as made" condition, in order to check the stability of the interface during the manufacturing procedure and to have a set of initial concentration profiles to be used as the reference state with which to compare the effect of any subsequent annealing. The results obtained showed that the initial interface is very stable, see Fig. 1; that is, there is a sharp drop in the concentration gradient as one moves across the interface. The Al signal in the SiC drops to about 2% its value in the matrix at a position no more than 10 nm across the interface; similar results were obtained for the Si and C signals as the beam was positioned 10 nm into the matrix. The interface was seen to be rather planar and clean with no voids

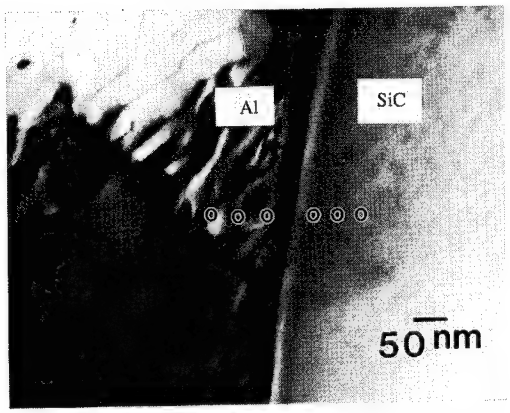

Fig. 1. TEM micrograph of "as made" SiC/Al composite. The interface is seen to be planar, free of any voids and clean (no precipitates or segregation).

present. This means that the bonding is strong and of an electrostatic nature (i.e. electronic or charge transfer bonding) with no interdiffusion present among the different components of the composite [14].

Once the reference state had been obtained, a comparison was then carried out with the annealed samples. There was no noticeable difference between the samples observed in the "as made" condition and those annealed at 590°C, irrespective of what the annealing time was (in some cases up to 1000 h). The interface was once again seen to be rather planar and clean, devoid of any segregation or any substantial interfacial reaction, similar to that of Fig. 1. Figure 2 is a linescan profile taken across this interface with a 10 nm diameter beam. The X-ray data was gathered at points 10 nm apart from each other with a lifetime acquisition of 500 s; even though this limited the total number of accumulated counts to around 700, it was found to be sufficient to obtain a qualitative profile of any desired concentration gradient. It is then seen that both the Al and Si profiles are similar to those found at the bulk regions of the matrix and the reinforcement, respectively. It is only within a 10 nm region away from the interface that any changes are observed and these are most probably caused by the spatial limitations of the microscope itself. Of course, it might be possible that any interdiffusion is constrained to within 10 nm from the interface, but then, we are not able to obtain any evidence confirming this possibility. Note that the beam was positioned at a distance of 10 nm away from the interface and this may explain the sharp drop observed in the concentration profiles between the two adjacent points across the interface itself. From these results, we can then conclude that there is no diffusion of Al into SiC at temperatures below 650°C (which was the compaction temperature), neither during the manufacturing process nor during any subsequent annealing; this being the case irrespective of the annealing time.

This, on the other hand, is not the case with samples that were in contact with a liquid Al matrix at 680°C for 600 min. These samples actually showed two types of interfaces; some which were similar to those observed at 590°C and showed no diffusion or any interfacial reactions and others, as can be seen from Figs 3 and 4, which showed that an extensive interfacial reaction had occurred. This reaction led to the appearance of interfaces with an extensive serrated or jagged profile that produced "spikes" of SiC protruding into the Al matrix. Actually, the reacted region can be seen by tilting the sample in such a direction that both the matrix and the reinforcement have a light contrast while the reacted region within the SiC has a dark contrast. X-ray analysis shows the Al concentration to decrease as the beam is moved along the interface until it reaches the inner boundary of the dark region; at this point, the Al concentration drops to about 2% of its bulk value and remains constant across the rest of the SiC particle. No statistical counting procedure has

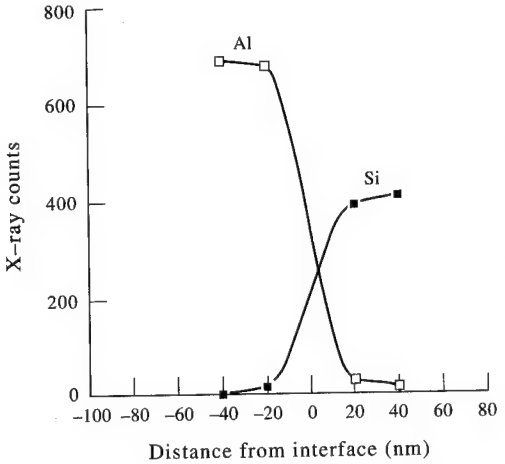

Fig. 2. Linescan profile across the interface of Fig. 1. There is a sharp drop in the Al and Si profiles across the interface. This is evidence of a lack of any interdiffusion.

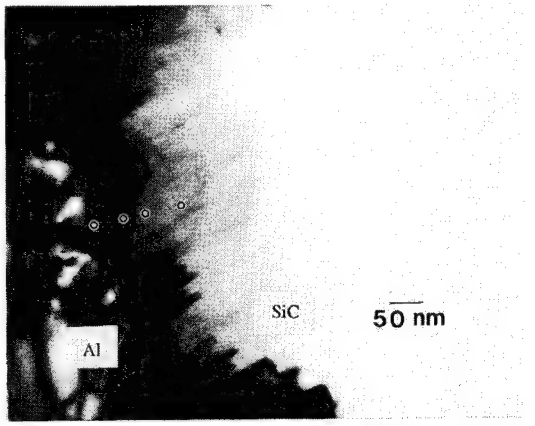

Fig. 3. Serrated interface of SiC/Al composite after annealing at 680°C for 10 h. The interface has now acquired a serrated shape evident of a substantial interfacial reaction that has dissolved the SiC.

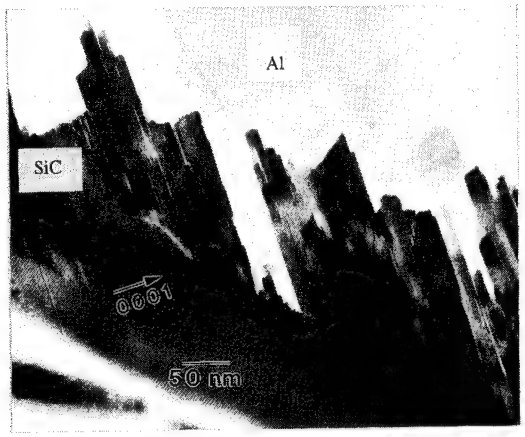

Fig. 4. Serrated interface of SiC/Al composite after annealing at 680°C for 10 h. Notice the irregularity of the serrated region and some of the cracks generated into the SiC.

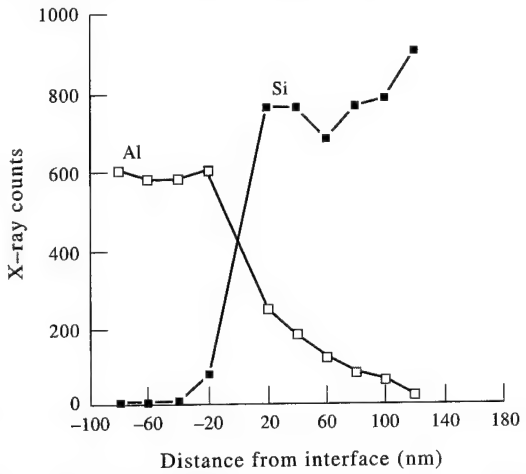

Fig. 6. Linescan profile taken across interface of Fig. 3. Note that the Al signal, 30 μm into the SiC, is about 25% that in the matrix. Such concentrations cannot be produced in their entirety by fluorescence of Al by Si X-rays.

yet been carried out in order to obtain the vol.% of these particles as a function of the total SiC population; but, it should be pointed out that these particles are not difficult to find in the observed areas so we can deduce that this is not just a simple occurrence on some selected particles but a more general effect throughout the sample.

Our present investigation showed the appearance of square-like crystals, see Fig. 5, which were identified, some as Al_2O_3 and some as $MgAl_2O_4$, but these were not found to be adhering to the SiC surface; in fact they were observed to form in the matrix at distances up to about 100 nm away from the interface. Even though the only available phase diagram for the Al–Si–C system shows that Al_4C_3 is the expected product of any reaction occurring at temperatures below 700°C [15–17], no Al_4C_3 was observed in these samples; this means that a thick mass of liquid Al was in contact with the SiC and a strong wetting bond was then present [17, 18].

Linescans profiles, as seen on Fig. 6, taken from the interface on Fig. 3 show substantial penetration of Al, up to about 100 nm into the SiC; in fact, up to about 25% Al is seen to be present within 25 nm from the interface. These concentrations are too large to have been produced by fluorescence of Al due to Si X-rays, while the absorption effect is considered to be small since very thin regions of the sample were used for all of the X-ray analyses. Linescan profiles were taken across a number of these serrated interfaces and similar results were obtained in all cases. The matrix side showed the Si concentration to be very small (i.e. ~2%).

Closer examination of some of the serrated surfaces, see Fig. 7, reveals the SiC being broken up by some of the Al actually penetrating in between some of the planes of these surfaces. Such an effect can also be observed in the concurrent bright and dark field images, as shown in Fig. 8, where substantial

Fig. 5. Precipitation of $MgAl_2O_4$, away from the interface, after annealing at 680°C for 10 h. This spinel, along with some Al_2C_3 were the only precipitates observed. Usually, these were found not to adhere to the interface.

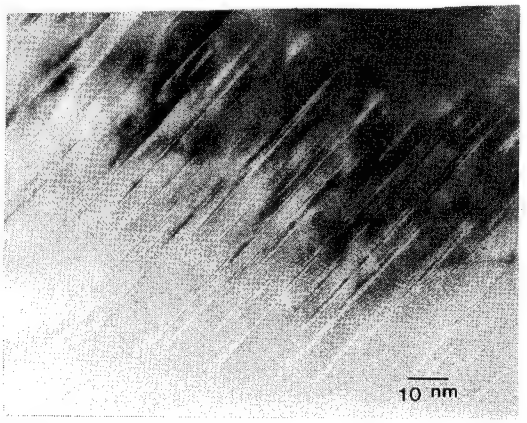

Fig. 7. Channel pattern in the "dark interfacial" region after annealing at 680°C for 10 h. These channels may be the result of the dissolution and reprecipitation of SiC in the matrix without the formation of Al_4C_3.

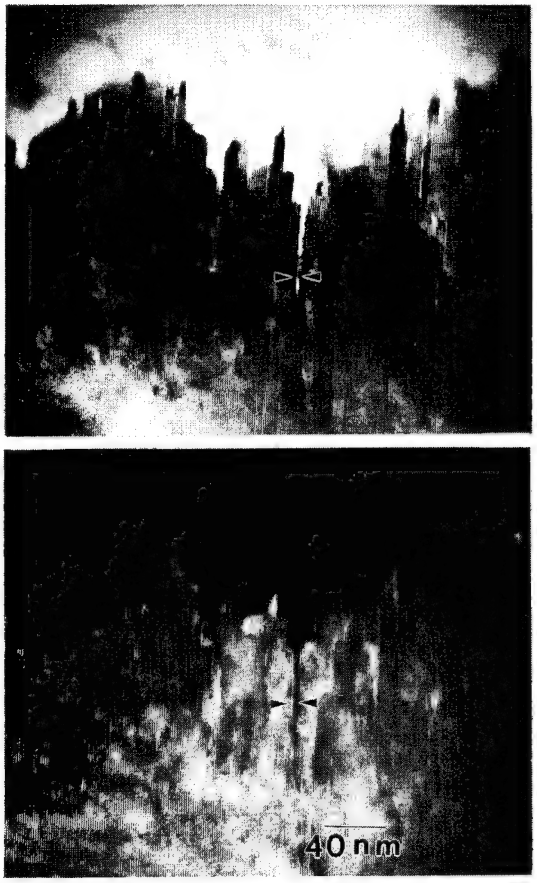

Fig. 8. Bright and dark field image of "dissolved" channels after annealing at 680°C for 10 h. The Al concentration in the channels can be as high as 50% that of the Si in the SiC.

amounts of Al can be seen to have penetrated in between some of the dissolving planes of the SiC. As the SiC dissolves, the Al "penetrates in" through these channels that open up (as shown by the arrow) and X-ray analyses taken from this region showed the Al concentration to be as high as 50% of the total count. The high resolution image, see Fig. 9, shows the 6H stacking of the SiC along the interface showing some of the faults in the stacking sequence that appear as the Al penetrates into the SiC.

The linescan profiles showing a concentration gradient, see Fig. 6, can then be the end result of two concurrent effects; one of them due to actual interdiffusion between Si and Al along the interface (by Al atoms replacing, in the SiC lattice, some of the Si atoms that have dissolved in the liquid matrix—note that up to 18 wt% Si is able to dissolve in Al at 680°C) and the other due to a penetration of the SiC crystal by Al as a result of the breaking of the SiC crystal through dissolution of some of its planes in the liquid matrix.

Diffraction patterns taken from the bulk of the SiC showed them to be similar to those taken from the "dark interfacial" region. The presence of Al was not observed in these patterns, but this is probably due to the extremely small regions in which Al is concentrated (i.e. the dissolved channels shown in Fig. 7) or, due to the possibility that Al may have diffused and formed a solid solution in SiC by replacing some of the Si atoms "lost" during the dissolution process. From these diffraction patterns, it can also be concluded that the serrated planes form along the basal planes of the SiC.

Of utmost interest was the sample annealed for only 3 min at 680°C. This sample also showed the appearance of two types of interfaces. In the majority of the interfaces in this sample no substantial reaction (i.e. a sharp planar interface was observed) was evident and, in these cases, the concentration gradients were similar to those of the "as made" sample. At the same time, a small fraction of the other interfaces showed the appearance of a small serrated profile in some localized positions along the length of the interface. X-ray analysis of these regions revealed the presence of Al in the SiC crystal, just as for those samples annealed for over 600 min at 680°C; the concentration being as high as 25% of the total X-ray count.

Linescan profiles taken from the samples which had been given an additional annealing at 590°C, after being in contact with liquid Al, showed no additional change in the concentration profiles or in the interfacial appearance. This then implies that any of the changes observed can occur only in the presence of a liquid matrix; any further annealing at temperatures below 650°C does not affect the interfacial chemical state of the composite.

DISCUSSION

The observed results can be due to two concurrent effects (i.e. penetration and/or diffusion of Al into SiC). It is difficult to experimentally differentiate between these two effects due to the constraints imposed by the spatial resolution of the microscope, which is of about 10–15 nm if a significant count rate is desired in a reasonable time, i.e. less than 5 min per point. Note, of course, that it is necessary to discontinue the X-ray analysis every 30 s in order to check that there has not been any shift in the position of the beam; this then makes the count rate at every point a very laborious procedure, which would worsen if a higher spatial resolution is required. The stability of the sample under such conditions must also be accounted for (i.e. on a couple of occasions, a hole was made through the thin regions of the sample and the analysis had to be discontinued). We will then discuss these two effects separately, followed by a general discussion.

Penetration

As was shown in Fig. 8, the reacted interface is composed of a number of channels made by the

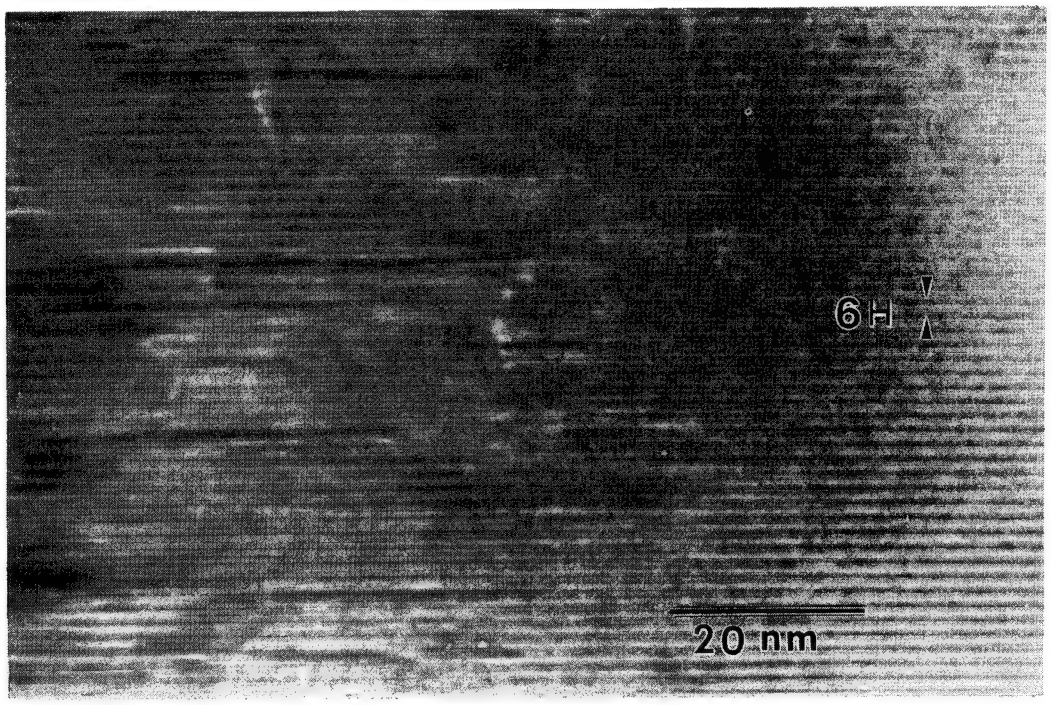

Fig. 9. HREM image of the interface showing the faults as Al penetrates into the SiC crystal.

penetration of liquid Al into the SiC lattice due to the respective dissolution of SiC into the liquid matrix. We can then state that our present results (i.e. significant Al penetration into SiC) are probably due to the SiC being thermodynamically unstable in the presence of liquid Al at 680°C; in fact, such a process (i.e. the dissolution of SiC without the formation of Al_4C_3) has already been proposed in the past, on a thermodynamic basis, by Kannikeswaran and Lin [19].

Notice that if this process were to occur, this would explain not only the lack of any substantial Al_4C_3, but it might also explain the channels observed in the serrated surfaces. As new SiC is being reprecipitated, some Al layers may be trapped in between the SiC crystals and this would then lead to the formation of the observed channels. The dissolution process is then at first rather inhomogeneous as the SiC is dissolved in the matrix from high energy sites along the interface and reprecipitated again along low energy sites on the interface; as the dissolution progresses, "spikes" of SiC are created or left over from the dissolution which are separated from each other by regions of Al with Si in solution and $MgAl_2O_4$ and Al_2O_3 precipitates a distance away into the matrix. The SiC/Al reaction at 680°C is then seen to occur not as a continuous planar reaction forming Al_4C_3 at the interface, but more like a discontinuous dissolution and reprecipitation reaction of the SiC along the basal planes. This type of reaction is favorable due to the strain present in the SiC, the large number of Si atoms that are able to rapidly dissolve in liquid Al at distances very close to the interface and to the use of a lower annealing temperature (i.e. below 700°C) which slows down the rate of formation of Al_4C_3.

The effect of two important variables must be noted with respect to the formation of Al_4C_3; these are: the concentration of Si in the Al matrix and the annealing temperature. It is well known that as the Si concentration in the Al matrix increases (i.e. its activity increases), the propensity of the composite to form Al_4C_3 decreases [20]. As the Si concentration reaches a value of about 10 wt% in the matrix, the amount of Al_4C_3 formed decreases substantially and it will eventually not form at all as the Si concentration goes to above 10 wt%. Thus, under the right conditions, it is possible to have SiC dissolve into a liquid Al matrix and not form Al_4C_3; this being possible as long as Si is able to dissolve in the matrix while still providing a barrier for the formation of Al_4C_3 and leading to the reprecipitation of SiC once again along the interface. The second factor to consider is the annealing temperature; as reported before [17], the amount of Al_4C_3 that forms in the Al–Si–C system is highly dependent on the annealing temperature. For example, at 680°C, only 0.0001 mol% Al_4C_3 is expected to form in a period of 10 h; this is in sharp contrast with the amount expected at 700°C, in which case, up to 0.004 mol% Al_4C_3 is formed in a period of less than 30 min (i.e. 40 times more than at 680°C). As the temperature is increased to 700°C and above, the amount of Al_4C_3 that forms approaches its saturation point so rapidly that any significant

interpenetration at the interface is hindered and the interfacial layer formed then acts as a barrier for any Al penetration into SiC.

The use of such a high temperature (for example, Porte [9] and Bermudez [10] annealed their samples at 800°C while Iseki *et al.* [15] used 1100°C as the annealing temperature) would then explain why previous investigators have not observed the serrated profiles presently reported since this causes the Al_4C_3 to form rather fast while the presence of impurities in the matrix leads to the formation, at the interface, of diffusion barriers that prevent any substantial interpenetration.

A rather pure matrix (i.e. the 1100 Al used in this investigation) allows for rapid and substantial amounts of Si to dissolve in the liquid matrix at distances very close to the interface (i.e. around 100 nm into the matrix); at 680°C, up to 18% Si is able to dissolve in liquid Al, while the amount of Al_4C_3 expected to form is very small. The amount of dissolved Si is not only enough to prevent the formation of Al_4C_3 (as expected from thermodynamic calculations), but it may also cause the consumption of the C atoms present in the matrix [19]. This is possible since the amount of Si in Al required to prevent the formation of Al_4C_3 is already available very close to the interface, even though the matrix, as a whole, may still show only a small concentration of Si which is more representative of the bulk matrix than of the interface between Al and SiC. Since we did not find any large concentrations of Al_4C_3, we then expect this to have been caused either by the very small amounts of Al_4C_3 formed (which may have gone undetected) or, more probably, to the reprecipitation of SiC in the Al matrix (along the interface) without the formation of Al_4C_3.

Diffusion

The second effect of the observed interfacial reaction may be due to the actual diffusion of Al into SiC by replacing the empty Si lattice sites generated due to the large amounts of Si that have dissolved in the liquid matrix. In this respect, it should be noted that previous work by Lucke *et al.* [21], has also shown how Al is able to diffuse into SiC when the SiC is heavily damaged or when Si vacancies are available due to surface oxidation. Such interpenetration (between Al and Si) is then dependent on the amount of Si that is able to dissolve in the Al matrix; as Si dissolves in the matrix, a similar amount of Al is then able to replace the "missing" Si atoms in the SiC lattice. This, then, means that it may be possible for Al to diffuse into the SiC lattice, but only as long as Si is also able to dissolve into the liquid matrix (i.e. there must be a concurrent interdiffusion effect at the interface between Al and Si). Of course, since no Si precipitates were observed in any of the samples, this possible explanation cannot account for our results. Thus, the diffusion of Al into SiC cannot contribute to the Al signal that appears in the serrated regions. The Al concentration observed in these regions must then come from the signal generated by the Al-containing channels formed during the dissolution of SiC.

General

These results differ somewhat from what has been reported in the past [5, 11, 22]. The work of Cao *et al.* [8] has shown a very stable interface between Al and SiC whiskers (i.e. no interdiffusion was found at the interface). The annealing temperature in this case, though, was not much higher than 660°C and the sample was probably not held at that temperature for a substantial amount of time. We have shown how only a very small percentage of the SiC particles react at this temperature so it is possible that the reacted particles might have been missed and no X-ray analysis taken across the whiskers that may have reacted; this, coupled with the results of Handwerker *et al.* [6], which show whiskers to be more stable than particulates, would then explain why no interfacial reaction was observed. The work of Dignard-Bailey *et al.* [22], was carried out on a SiC particulate Al-2014 composite. The composite was bought from a commercial source and no details of its manufacturing steps are known, although it is believed that the matrix was in the liquid state. Subsequent annealing treatments were all kept below 500°C. The interface was seen to be planar and three main intermetallic phases were observed. Some of the interfaces also had a serrated shape and some Al penetration was observed, which is similar to what we observed. The percentage of these serrated interfaces was reported to be small, while the extent of Al penetration was not reported as a function of distance from the interface. The presence of different interfacial layers may have contributed to the small amount of Al penetrating in the SiC. This might be the case since these layers will not only act as diffusion barriers, but will also (by reacting with Al) remove any Al that might be free to penetrate into the SiC. The work of Arsenault and Pande [11], on the other hand, consisted of two parts: an Auger linescan analysis across a polished section of a SiC particulate in an Al matrix and an STEM analysis of a SiC-particulate/Al composite. Part of this work may have been the result of experimental artefacts; for example, the linescan signal obtained from the polished sample could also have come from some Al layers lying underneath the particle and contributing to the profile obtained (note also that the spatial resolution in such a case is of about 2 μm). On the other hand, it might be possible that the STEM part of the investigation may actually be showing real results similar to what we currently found in some of the planar interfaces (i.e. some Al penetration even if the interface was planar, as long as the matrix was in the liquid state).

We, therefore, believe that our results do show a substantial interpenetration effect that does not

involve the diffusion of Al into SiC; we expect the interpenetration observed to be due to the presence of stresses in the SiC leading to the formation of high energy sites along the interface, which then aid the process of dissolution as proposed by Handwerker *et al.* [6] and as previously observed during the growth of crystals [23]. In these cases, the Mo–Ni and the Mo–Ni–Fe interfaces were found to be stable in the solid state, but underwent rapid interdiffusion as the matrix reached the liquid state [6]. Bhat *et al.* [23] found that the retained elastic strain of crystals, which had been previously fractured, caused the subsequent regrowth rate of such crystals to decrease due to the higher solubility of the solute (which was being used as a dopant) in the growing crystal as a function of strain; that is, as the retained strain was removed, the solubility of the solute in the growing crystal decreased and the subsequent regrowth rate of the crystal increased. Such an effect has also been observed in the interdiffusion of Al deposited onto thin films of epitaxially grown Si; that is, as the strain of the thin film was removed,the interdiffusion depth decreased from around 100 nm to less than 10 nm at temperatures of between 400 and 600°C [24]. Handwerker *et al.* [6] observed how a liquid will have a different equilibrium composition with a stressed solid than with an unstressed solid; in order to achieve equilibrium, the stressed solid will dissolve in the liquid while the liquid will concurrently diffuse into the solid. The subsequent coherency stresses generated during the diffusion process, due to the atomic size mismatch, will cause the interface to attain a serrated shape due to the continuous dissolution and reprecipitation processes that occur simultaneously. In places where the solid is stressed, a dissolution process will take place; on the other hand, in places where the solid is relieved of stresses, the solid will be reprecipitated along the interface.

In our case, the stresses in the SiC may arise either from the residual lattice strain imposed upon the SiC surface due to the ball milling operations the SiC has been subjected to [25]; or, due to the rapid dissolution of Si in liquid Al that allows the Al to penetrate into the SiC, thereby generating coherency stresses that lead to an unstable state at the interface and to its serrated shape due to the subsequent reprecipitation of SiC. It has actually been found that the stresses developed by the ball milling operation have the same results (i.e. an increase in the solubility of the solute in the growing crystal) as those obtained from the retained elastic strain due to fracture [23]. This is in accord with results obtained for the dissolution of SiC in liquid Si, in which the dissolution of SiC was observed to be a function of the rate at which C atoms were removed from the interface [26]. As the C removal rate slowed down, the dissolution of SiC also decreased since the Si atoms were not able to diffuse away from the interface.

CONCLUSIONS

The following conclusions can be reached based on the present investigation:

1. The SiC/Al interface is chemically stable at temperatures below 650°C and this prevents the diffusion of Al into SiC at these temperatures.
2. There is a substantial dissolution of SiC, along the basal planes, in the presence of a liquid Al matrix.
3. At temperatures above 660°C but below 700°C, the SiC crystal takes a serrated surface shape as it reacts with liquid Al and this leads to a significant penetration of Al into SiC along the channels formed at the serrated interfaces.
4. Diffusion of Al into SiC was not expected to occur even in those interfaces that had undergone a substantial reaction leading to a serrated shape.
5. Al_4C_3 was not observed to have formed at temperatures below 700°C and this is expected to be due to the dissolution of SiC from high energy sites along the interface and its reprecipitation once again at low energy sites. Above 700°C, the amount of Al_4C_3 formed increases so rapidly and at a much faster rate so that any possible diffusion is prevented by the formation of an interfacial layer.
6. After the initial interpenetration in the liquid state, annealing at temperatures lower than 650°C has no effect on the chemical state of the composite.

Acknowledgements—We would like to acknowledge the help of Dr L. Wang and Mr Gene Taylor during the analysis of the TEM work and the helpful discussions with Dr Y. R. Mahajan in identifying the spinel precipitates. We would also like to acknowledge the continued support of Dr S. Fishman of the Office of Naval Research under contract N 00014-91-J-1353.

REFERENCES

1. D. McDanels and C. Hoffman, NASA Technical Paper #2302 (1984).
2. R. J. Arsenault and R. M. Fisher, *Scripta. metall.* **17,** 67 (1983).
3. M. Vogelsang, R. J. Arsenault and R. M. Fisher, *Metall. Trans.* **17A,** 379 (1986).
4. R. J. Arsenault and N. Shi, *Mater. Sci. Engng* **81,** 175 (1986).
5. R. J. Arsenault, L. Wang and C. R. Feng, *Acta metall.* **39,** 47 (1991).
6. C. A. Handwerker, J. W. Cahn and J. R. Manning, *Mater. Sci. Engng A* **126,** 173 (1990).
7. Y. Tajima, K. Kyima and W. D. Kingery, *J. chem. Phys.* **77,** 244 (1982).
8. L. Cao, L. Cheng, C. K. Yao and T. C. Lei, *Scripta metall.* **23,** 227 (1989).
9. L. Porte, *J. appl. Phys.* **60,** 635 (1986).
10. V. Bermudez, *Appl. Phys. Lett.* **42,** 70 (1983).
11. R. J. Arsenault and C. S. Pande, *Scripta metall.* **18,** 1131 (1984).
12. S. R. Nutt and R. Carpenter, *Mater. Sci. Engng* **75,** 1131 (1984).
13. M. Strangwood, C. A. Hippsley and J. J. Lewandowski, *Scripta metall.* **24,** 1483 (1990).
14. S. Li, R. J. Arsenault and P. Jena, *J. appl. Phys.* **64,** 6246 (1988).

15. T. Iseki, T. Kameda and T. Marayuna, *J. Mater. Sci.* **19,** 1692 (1984).
16. V. Laurent, D. Chatain and N. Fostathopoulos, *J. Mater. Sci.* **22,** 244 (1987).
17. J. C. Viala, P. Fortier and J. Bouix, *J. Mater. Sci.* **25,** 1842 (1990).
18. S. Y. Oh, J. A. Cornie and K. C. Russell, *Metall. Trans.* **20A,** 533 (1989).
19. K. Kannikeswaran and R. Y. Lin, *J. Metals* **9,** 17 (1987).
20. J. C. Ehrstrom and W. H. Kool, *J. Mater. Sci.* **23,** 3195 (1988).
21. W. Lucke, J. Comas, G. Hubler and K. Dunning, *J. appl. Phys.* **46,** 944 (1977).
22. L. M. Dignard-Bailey, T. F. Malis, J. D. Boyd and J. D. Embury, *Proc. Int. Symp. on Advanced Structural Materials.* Pergamon Press, Toronto (1988).
23. H. L. Bhat, J. N. Sherwood and T. Shripathi, *Chem. Engng Sci.* **42,** 609 (1987).
24. L. J. Brillson and M. L. Slade, *Appl. Phys. Lett.* **44,** 110 (1984).
25. Y. Kano, *Powder Tech.* **44,** 93 (1985).
26. W. P. Minnear, *J. Electrochr. Soc.: Solid St. Sci. Tech.* **226,** 634 (1979).

Pergamon

Scripta Metallurgica *et* Materialia, Vol. 32, No. 11, pp. 1783-1787, 1995

0956-716X/95 $9.50 + .00

0956-716X(95)00008-9

A COMPARISON OF INTERFACIAL ARRANGEMENTS OF SiC/Al COMPOSITES

R. J. Arsenault and J. C. Romero
Metallurgical Materials Laboratory
Department of Materials and Nuclear Engineering
University of Maryland, College Park, MD, 20742 - 2115

(Received November 10, 1994)
(Revised December 19, 1994)

Introduction

The importance of a strong bond at the interface in composites in terms of the strengthening observed can not be understated, whether the mechanism of strengthening is load transfer or work hardening of the matrix due to the relaxation of the thermal stresses. It has been shown experimentally [1] and theoretically [2] that bond strength between SiC and Al can be very large. However, there is no consensus as to the orientation relation (OR) at SiC/Al interface even though in most cases it is atomically sharp. If the composite is made by hot compaction of powders or hot pressing of layers of SiC and Al then an amorphous phase [3,4] appears, but if substantial plastic deformation of a powder compact of SiC and Al occurs then random OR are found [1,5], and in one case a specific OR was reported [6], which is the same OR assumed by Li et al. [1], but in the same composite system [7], no specific OR was found. Finally if the matrix was molten during processing, two specific OR were reported [8,9].

If the matrix is in the molten state during processing, then more than likely that a consistent OR would occur. This OR would also most likely have a low strain energy. The purpose of the present investigation was to determine if a consistent OR was obtained in a molten matrix SiC/Al composite.

Experimental Procedure

The present investigation was carried out on composites prepared in the following manner. To insure a relatively homogeneous distribution of SiC within the Al matrix, an 1100 Al powder was mixed with 20 V% SiC platelets of the α-6H structure. The SiC platelets had a maximum dimension of 5 μm. The mixing technique is discussed elsewhere [10]. The powder samples were vacuum hot compressed at 550°C for 1 hour and then allowed to furnace cool under pressure after which they were extruded at 500°C with a reduction ration of 8:1. Cylindrical samples were then cut from these composites (12.5 mm in diameter and 12.5 mm in length) and finally these samples were heated at 680°C for 10 hours and furnace cooled in order to insure that the Al matrix was in the liquid state. The TEM samples were prepared by core drilling a 3 mm diameter disc from a 0.5 mm thick slice cut by electrical discharge machining at low power from each of the samples. The discs were then dimpled, from one side only, with a 30 μm diamond paste until the thickness at the center of the disc was about 50 μm. The final step involved an ion milling operation which was carried out in a TECHNICS IV Ion Mill using an Ar^+ gas set at 4 kV and at an angle of 20° to the sample. Once perforation

was achieved, the angle was lowered to 10° and the ion milling was continued for another 30 minutes in order to obtain a thin region over a wider area.

Results

To obtain suitable HREM images, the matrix and reinforcement, across each side to the interface, must be oriented in such a way that both have a low index zone axis which is parallel to the electron beam. The $[11\bar{2}0]$ zone axis of SiC was chosen so that the SiC basal planes would be parallel to the interfacial plane. The [110] zone axis of Al was used due to the requirement of not only observing the (111) Al planes but also of keeping the diffraction condition previously set on the SiC. In order to obtain the necessary HREM images, it was necessary to concentrate on very thin regions of the samples and to orient the sample in such a way that the useful diffraction conditions were obtained in both the matrix and the particle. This was sometimes difficult due to the different ion milling rates of the matrix and reinforcement. This difference in the milling rates may cause a change in the thickness present at both sides of the interface and can lead to the formation of an edge or step at the interface. The thickness of the sample, as well as the formation of this step which may generate a white contrast observed at the interface, created conditions detrimental to HREM so that not all the interfaces were useful even if the required diffraction conditions were met. The HREM image obtained, see Fig. 1, shows only one set of (111) planes. This is due to a small tilt away from the [110] axis. It was not possible (or we were not able) to obtain better images due to the constraint on the amount of tilting in the microscope; thus, the thinnest regions of the samples were not necessarily available for HREM and we obtained the best possible images under these circumstances. Our point, though, was to see if the (111) planes align parallel to the (0001) panes of SiC. In all the cases observed, the (111) planes were seen to align themselves at 20° to the basal planes.

The results obtained in this investigation show that there is an orientation difference between the adjoining interfacial planes, such that the (111) planes of the Al are oriented at 20° to the (0001) planes of the SiC, see Fig. 1. The crystallographic relationship obtained in this investigation is then deduced to be given by :

$$[11\bar{2}0] \parallel [110], \quad (0001) \parallel (112)$$

Figure 1, which was typical of what was found, then, shows two things. First, the interface is clean and continuous. If the interface is examined very closely, the SiC is not exactly parallel to the (0001). It is possible to have some (0001) planes terminating at the interface, as indicated by the arrow in Fig.2. This termination may be defined as a "step". Even though the area shown on Fig. 1 is rather small, it should be noted that this image was magnified in order to show better detail; Fig. 2 shows the same area at a lower magnification and

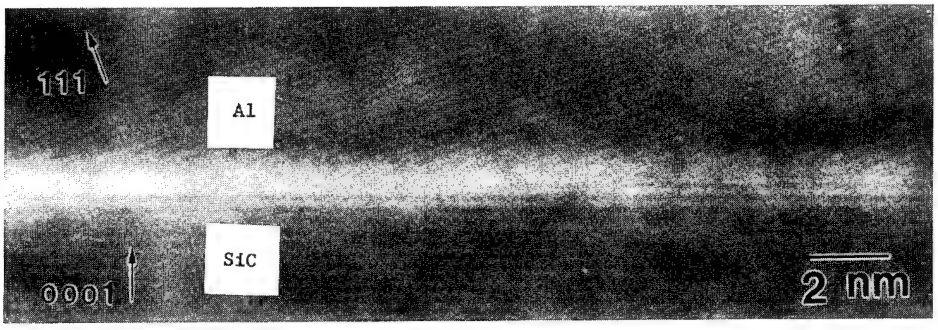

Figure 1. It can be seen that the (111) planes are aligned at 20° to SiC basal planes which means that the (112) Al planes are parallel to the basal planes.

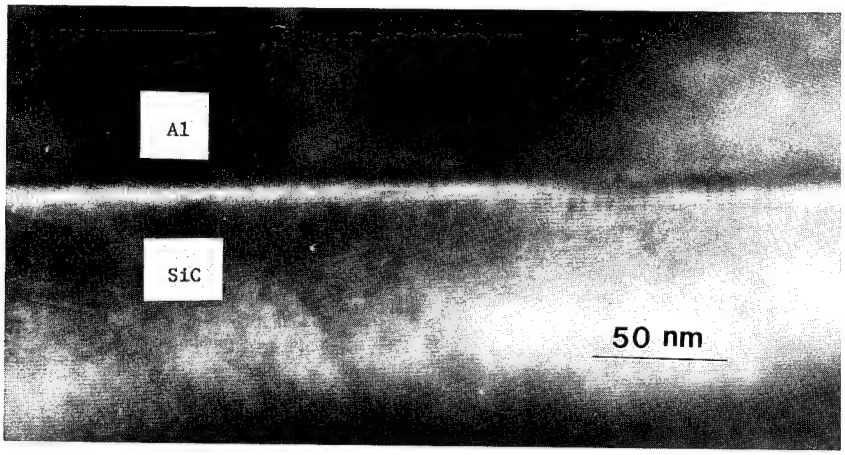

Figure 2. A precipitate and amorphous free interface. Such an interface appears to be stepped at a small angle.

the same observations can be made. Second, the (111) Al planes are oriented at 20° to the basal planes of the SiC; this, then, implies that the (112) Al planes are parallel to the basal planes although the (112) planes could not be directly observed due to the resolution limits of the microscope (i.e. the (112) interplanar spacing is much smaller than the point to point resolution of the microscope).

Discussion

A stereoprojection of the $[11\bar{2}0]$ and [110] poles of the SiC and Al, respectively, was then prepared in order to obtain other possible crystallographic relationships in the SiC-Al system (where a_{Al} = .405 nm; a_{SiC} = .307 nm and c_{SiC} = 1.503 nm). Once these stereoprojections were obtained, the [110] Al plot was superimposed onto the $[11\bar{2}0]$ SiC plot with the [111] Al pole on top of the [0001] SiC pole. This [111] Al pole was then rotated 20° (since this was the experimentally obtained condition) and the new alignment was checked to see which are the poles, from Al and SiC, which coincide with each other. As can be seen, see Fig. 3, not only do the (112) Al planes coincide with the (0001) SiC planes (which is the relationship observed in this investigation), but the following variant relationship can also be observed: $[11\bar{2}0]\|[110]$, $(01\bar{1}0)\|(111)$.

This last orientation relationship is the one reported by Weimin et al. [8]. At the same time, the relationship reported by Carim [9] (i.e. $[11\bar{2}0] \| [110]$, $(1\bar{1}01)\| (557)$ - note, though, that the Al plane is not in a low index relationship), appears to be another variant of the same OR, although there is now a slight misalignment of about 2° between the two poles when this relationship is checked against the stereoprojections on Fig. 3. Thus, the two other crystallographic relationships reported by Weimin et al. [8] and Carim [9] are the variants, obtained by the stereoprojections mentioned above, of the crystallographic relationship presently observed.

In regards to the possible "stepped" interface, it should be pointed out that the "step" occurs in the SiC. This means that the step was present before the interface formed and this further means that the formation of the step is not related to the reduction of the energy of interface.

If we consider a hard sphere model, without atom relaxation, (This assumption was valid for the calculation of dislocation spacing at Al_2O_3/NiAl interface [11].) for the (0001)SiC‖(111)Al, the strain generated is 7.34% as can be seen below:

$$\delta = \frac{d_{SiC}^{[11\bar{2}0]} - d_{Al}^{[110]}}{d_{Al}^{[110]}} = \frac{.307 - .286}{.286} = 7.34\%$$

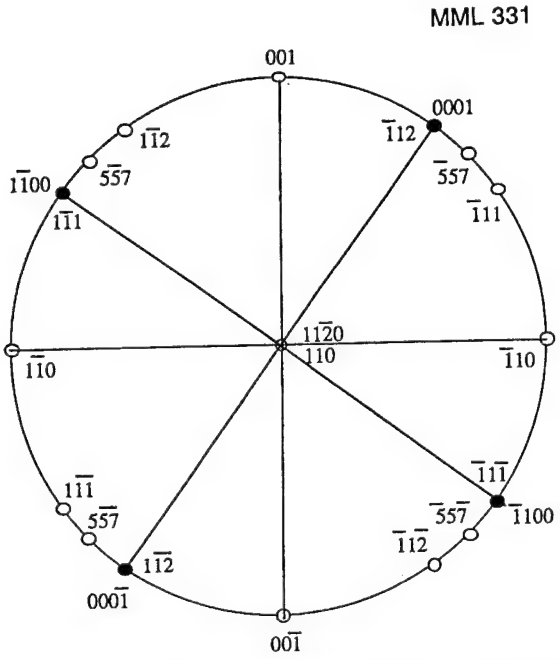

Figure 3. Stereoplots of Al and SiC along the [11$\bar{2}$0] and [110] directions showing the crystallographic orientation relation-ships that are possible in this system. The black circles rep-resent those poles which are coincident for both systems. The SiC plot has been tilted 20° with respect to that of the Al pole (after the (111) pole was placed on top of the (0001) pole).

In Fig. 4, the lattice constant of the basal planes of SiC is matched to the horizontal distance separating each Al atom in the (112) planes by considering the ABC stacking sequence of the (111) Al planes. This horizontal distance is of $d^{[110]}_{Al}/\cos(20^\circ) = 0.304$ nm and leads to a strain of only 0.98 %, as shown below:

$$\delta = \frac{d^{[11\bar{2}0]}_{Sic} - d^{[110]/20^\circ}_{Al}}{d^{[110]/20^\circ}_{Al}} = \frac{.307 - \left(\frac{.286}{\cos(20^\circ)}\right)}{\left(\frac{.286}{\cos(20^\circ)}\right)} = 0.98\%$$

It is obvious there is a significant reduction in the lattice misfit strain in the case of the (0001)SiC|| (112)Al interface, and this is the most likely reason why this OR forms instead of the (0001)SiC||(111)Al interface. Also, as stated before, consistent OR are obtained when the matrix is in the molten state during processing, and the reason for this consistency is the freedom for epitaxial formation of an interface with the lowest lattice misfit strain energy.

Summary

The data indicates that if the matrix is in the molten state there is a consistency between the results of previous investigations [8,9] and the present investigation. We suggest then that the lowest interfacial energy OR is the following:

[11$\bar{2}$0] SiC || [110] Al; (0001) SiC || (112) Al;

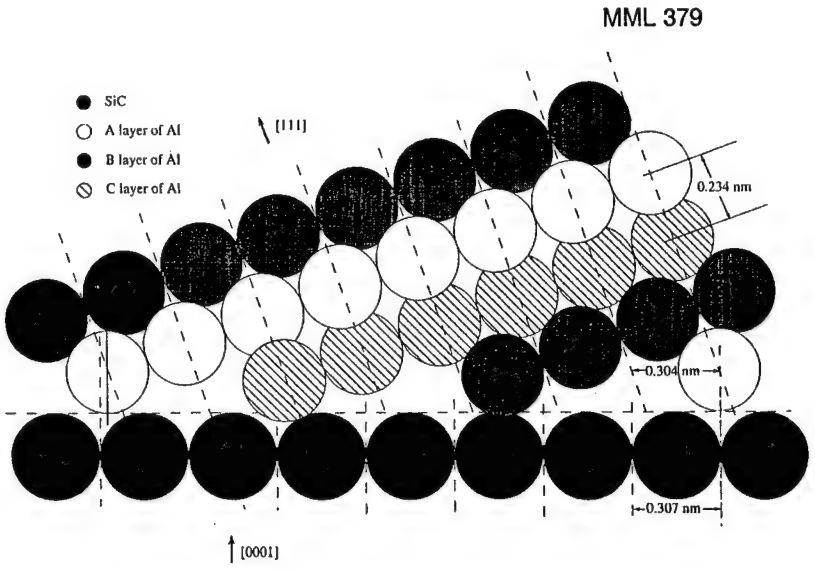

Figure 4. Schematic of the atomic packing at the (112)Al‖(0001) SiC interface. The rotation of the (111)Al planes by 20° away from the interface may be necessary not only to reduce the interfacial strain but also to increase the atomic matching con-figuration.

Acknowledgments

We would like to acknowledge the assistance and helpful discussions of Dr. L. Wang in obtaining the HREM images and the stereoplots and also the continued support of Dr. S. Fishman of the office of Naval Research under contract N 00014-94-10118.

References

1. Y. Flom and R.J. Arsenault, Mater. Sci. & Eng., 77, 191 (1986).
2. S. Li, R.J. Arsenault and P. Jena, J. Appl. Phys., 64, 6246 (1988).
3. S.R. Nutt, J. Am. Ceram. Soc., 71[3], 149 (1988).
4. P.L. Ratnaparkhi and J.M. Howe, Acta Met., 44, 811 (1994).
5. R.J. Arsenault, L. Wang and C.R. Feng, Acta Metall., 39, 47 (1991).
6. M. Van Den Burg and J.Th. M. De Hosson, Acta Metall., 40, S281 (1992).
7. V. Radmilovic, G. Thomas and S.K. Das, Mater. Sci. and Eng. A132, 171 (1991).
8. S. Weimin, L. Pengxing and L. Geyang, Composites: Design, Manufacturing and Application, ICCM/VIII; ed. by S. Tsai and G. S. Springer, Stanford University, SAMPE, 19-k-1 (1991).
9. A.H. Carim, Mat. Lett., 12, 153 (1991).
10. Y. Flom, Master thesis, University of Maryland, College Park, MD 20742, (1984).
11. L. Wang and R.J. Arsenault, Metall. Trans., 22A, 2617 (1991).

Interfaces in Continuous Filament-Reinforced Al_2O_3/NiAl Composites

L. WANG, K. XU, R.R. BOWMAN, and R.J. ARSENAULT

Interfacial structures in a continuous Al_2O_3 filament-reinforced NiAl composite were investigated by transmission electron microscopy (TEM). A graphite phase, which is an artifact of the composite fabrication procedure, decorates the interfacial region of the composite. The presence of the graphite is believed to play a role in both the low interfacial bond strength in the as-fabricated composite and the further reduction in bond strength after 10 thermal cycles in the temperature range of 373 to 1373 K. In regions where the graphite phase was not present, there appeared to be an intimate bond between the NiAl matrix and the Al_2O_3 filaments. Simulation of TEM diffraction contrast images based upon a three-dimensional (3D) finite element analysis was employed to investigate the nature of the residual strains in regions along the interface. The simulations suggested that radial residual strains within the Al_2O_3 filaments were randomly distributed along the interface. These strains are believed to be related to dislocation nucleation in the NiAl, which results from the relaxation of the thermally generated residual stresses.

I. INTRODUCTION

THE use of continuous filaments as composite reinforcements is currently being considered as a means of improving the creep resistance of intermetallics. In particular, it has been demonstrated that single-crystal Al_2O_3 filaments are capable of improving both the creep and fatigue resistance of NiAl.[1] The interfacial bond strength, which is strongly dependent upon the processing methods, plays a key role in the control of the mechanical properties of these continuously reinforced composites.[1] The strength of the interfacial bond is important because it strongly influences the thermal residual stresses (TRS), which develops during cooling due to the coefficient of thermal expansion (CTE) mismatch between the filaments and the matrix. In a previous investigation,[2] it was found that if an Al_2O_3/NiAl composite with an as-fabricated interfacial bond strength (measured by push-out testing) in the range of 90 to 180 MPa was thermally cycled 10 times in a temperature range of 373 to 1373 K, matrix cracking occurred. On the other hand, cracks were not observed after identical thermal cycling in those samples that had an interfacial bond strength in a range of 35 to 120 MPa. Also, the interfacial bond strength of these weakly bonded samples dropped to 5 to 30 MPa in the post-thermal-cycled condition. The mechanism(s) responsible for the difference in interfacial bond strength was not clear. It was also confirmed that the NiAl matrix was plastically deformed as a result of the relaxation of the TRS. Although dislocation densities in the region adjacent to the interface were found to be very high, dislocation generation in the interface region was not necessarily related to the interfacial bond strength since dislocation activity was observed in both weakly and strongly bonded composites.

In the present study, an electron microscopy investigation was undertaken to determine the interface structures of the single-crystal Al_2O_3 filament-reinforced NiAl composites that had a relatively weak interfacial bond strength, *i.e.*, 35 to 120 MPa, and the effect of thermal cycling on the interface structure of the composites. Simulations of transmission electron microscopy (TEM) diffraction contrast images based upon a three-dimensional (3D) finite element method (FEM) analysis were generated to understand the residual strain at regions adjacent to the interface.

II. MATERIALS AND EXPERIMENTAL METHODS

The composites used in this investigation consisted of a stoichiometric NiAl matrix unidirectionally reinforced with six plies of 125-μm diameter, *c*-axis oriented, continuous, single-crystal Al_2O_3 filaments comprising 30 vol pct of the composite; the matrix was fabricated from 50- to 150-μm diameter vacuum atomized prealloyed powders obtained from Homogeneous Metals, Inc., Clayville, NY. The Al_2O_3 filaments were supplied by Saphikon Inc., Milford, CT. The composites were fabricated using the powder-cloth (P-C) technique.[3] In this process, the matrix material is processed into flexible clothlike sheets by combining matrix powders with a fugitive organic binder. Likewise, fiber mats were produced by winding the fibers on a drum and applying another organic binder. The composite panel was assembled by stacking alternate layers of matrix cloth and fiber mats. This assemblage was consolidated by hot pressing followed by hot isostatic pressing (hipping) to ensure complete densification of the composite. After hipping, the steel containment can and Mo cladding required in the consolidation process were removed by

L. WANG, formerly Graduate Student, Department of Materials and Nuclear Engineering, University of Maryland, College Park, MD 20742-2115, is Senior Materials Engineer, Code 313/Materials Branch, GSFC/NASA, Greenbelt, MD 20771. K. XU, Graduate Student, and R.J. ARSENAULT, Professor and Director, are with the Department of Materials and Nuclear Engineering, Metallurgical Materials Laboratory, University of Maryland, College Park, MD 20742-2115. R.R. BOWMAN, Research Engineer, is with NASA Lewis Research Center, Cleveland, OH 44135.

Manuscript submitted June 21, 1994.

chemical etching in a bath of 45 pct nitric acid, 45 pct water, and 10 pct sulfuric acid. The resulting composite plates measured 15.2-cm long by 5.1-cm wide and 0.3-cm thick. Monolithic NiAl samples were processed by hot pressing followed by hipping NiAl powders (using no binders) at the same temperatures and pressures used for the composites.

The composites were annealed at 1473 K for 4 hours followed by furnace cooling. Ten thermal cycles were conducted between 373 and 1373 K with a heating rate of ~4 K/min, a 1-hour hold at 1373 K, then furnace-cooled to 373 K. Both the annealing and thermal cycling were conducted in a vacuum of $\sim 10^{-5}$ torr. The TEM samples of monolithic NiAl were produced *via* the dimple grinding plus an electropolishing method. Polishing was performed in a solution of 5 pct perchloric acid + ethanol at ~253 K with an applied voltage of 50 to 70 V. The cross-section Al_2O_3/NiAl TEM samples were prepared by dimple grinding plus ion milling, as described elsewhere.[4] The hole in the TEM foil was at approximately 1/2 the thickness of the composite plate, in other words, it was approximately 0.15 cm from the top surface of the plate. The plane of the foils were parallel or perpendicular to the filaments.

The TEM and X-ray energy dispersive spectra (EDS) analyses were performed on a JEM 2000-FX analytical electron microscope equipped with a Noran Voyager system. The foil thickness used in the calculation of the diffraction contrast image was measured by convergent beam electron diffraction (CBED) method.[5,6] From this data, it is also possible to obtain the extinction distance (ξ_g) by use of the EMS software program. An ABAQUS FEM software package was used to simulate the interface displacements. In the simulation of misfit interfacial dislocations, a simple FORTRAN program was used to calculate the displacements. The programs used for diffraction contrast simulation of TEM images were written in Interactive Data Language (IDL) running on a Sun workstation system.

III. EXPERIMENTAL RESULTS

A. *Decorated Interfaces*

A discontinuous graphite phase was frequently observed at the Al_2O_3/NiAl interfaces and grain boundaries in both the as-processed and thermally cycled composites. The graphite phase was not observed in the monolithic NiAl. The existence of the graphite phase in the composite has been confirmed by EDS, electron diffraction, and high-resolution electron microscopy (HREM). The graphite phase in the interfacial regions was generally island shaped. The size of the graphite phase ranges from submicron to a few microns, the distribution of the graphite was not homogeneous along the interface. A quantitative determination of the graphite islands density was not made, but there was no difficulty in finding the graphite islands. In the as-processed Al_2O_3/NiAl composite, as shown in Figure 1, the graphite phase appeared to be well bonded with matrix and Al_2O_3 filament.

After 10 thermal cycles of the composite plates, however, the graphite-decorated interface was usually debonded and deformation damage of the graphite phase became evident, as shown in Figure 2. About one-half of the examined Al_2O_3 filaments in all cross-section TEM samples of the composites were partially separated from the matrix after thermal cycling of the bulk composite plates. When gaps were observed between the filament and matrix, they were always associated with deformation damage of the graphite phase.

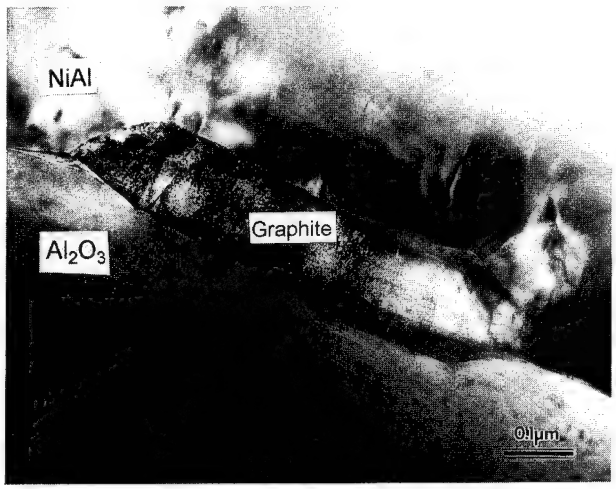

Fig. 1—TEM micrograph of a graphite-decorated interface between the single-crystal Al_2O_3 filament and the NiAl matrix, as-processed condition.

B. *Nondecorated Interfaces*

There were large areas where the interface was "clean," *i.e.*, free of any graphite decorations and other precipitates, as shown in Figure 3(a). Debonding was rarely observed at the clean interfaces either under the as-processed condition or after 10 thermal cycles. There were no consistent crystallographic orientation relationships between the filaments and matrix; *i.e.*, the orientations between the filament and matrix were random.

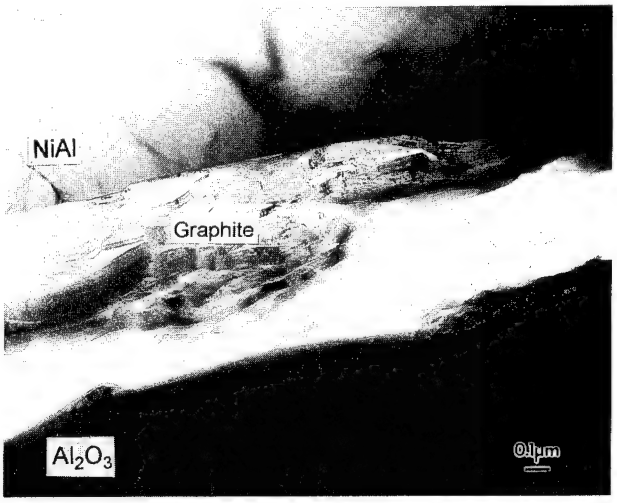

Fig. 2—TEM micrograph of a graphite-decorated interface between the single-crystal Al_2O_3 filament and the NiAl matrix, after 10 thermal cycles.

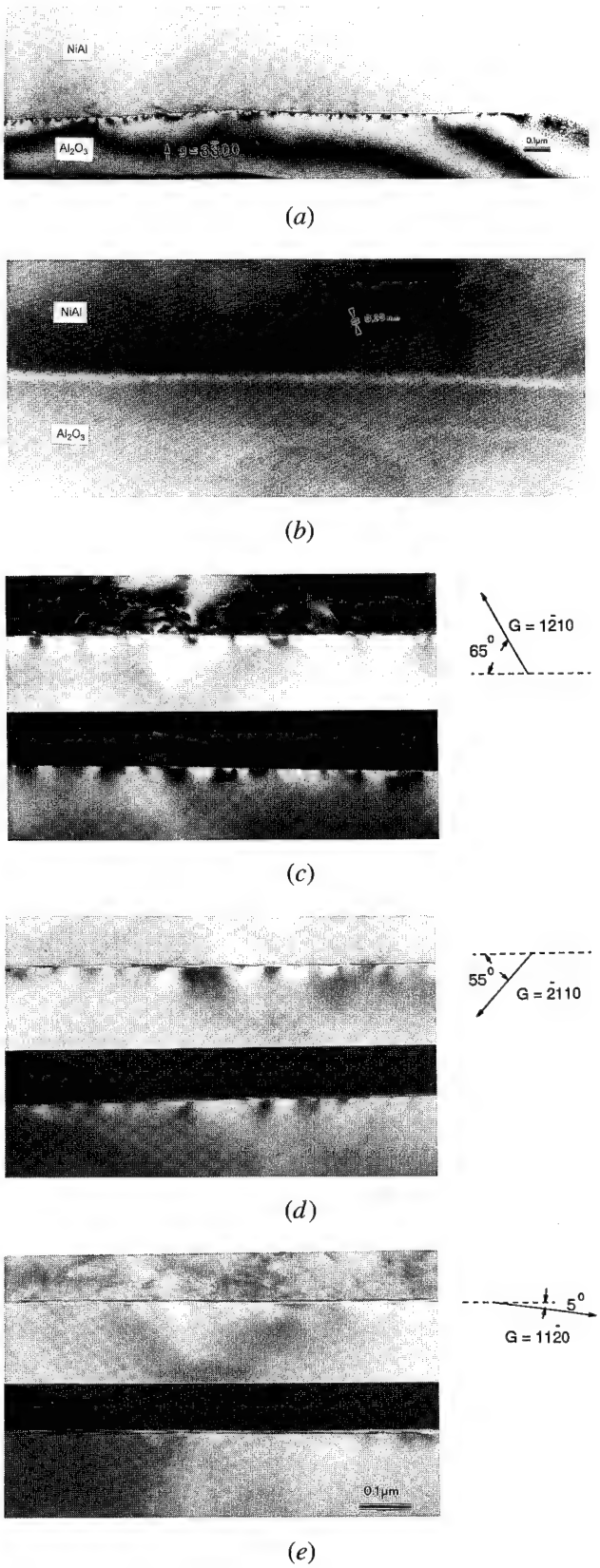

Fig. 3—TEM micrographs of a clean interface between the single-crystal Al_2O_3 filament and the NiAl matrix, after 10 thermal cycles: (*a*) the inhomogeneous diffraction contrast observed along the interface on the Al_2O_3 filament side; (*b*) HREM micrograph of the very thin area in (a); and (*c*) through (*e*) bright-field (top) and dark-field (bottom) images of the interface with different operating diffractions, $t = 1.3\xi_g$ with $\mathbf{g} = 11\bar{2}0$.

Neither coherent nor semicoherent interfaces were observed between the filament and matrix. However, HREM investigations of the clean interface indicated that the matrix and filament formed direct contact without noticeable intermediate layer or precipitates, as shown in Figure 3(b). It is likely that a randomly direct bond between the Al_2O_3 filament and the NiAl matrix has been achieved on an atomic level at the clean interface.

An unusual observation is that diffraction contrast in the Al_2O_3 filament at the interface was not homogeneous, but rather, modulated randomly along the clean interface, as shown in Figure 3(a). (There were no corresponding contrast images in the NiAl.) The wavelength of the modulation is around 0.1 μm. The foil thickness in this region in Figure 3 was ~220 nm, which was $\sim 1.3\xi_g$ of $\mathbf{g} = 11\bar{2}0$ of Al_2O_3. The modulated diffraction contrast disappears in regions where the foil thickness was less than a two-beam extinction distance with operating diffraction vector of $\mathbf{g} = 3\bar{3}00$, which is less than 95 nm. Different operating diffraction conditions were applied to produce different two-beam diffraction contrast images of the interface area, as shown in Figures 3(c) through (e). According to an analysis of these images, two important features were observed. First, minimum diffraction contrast was obtained when the diffraction vector was almost parallel to the interface (Figure 3(e)); second, the shape of the dark and bright areas of the image always tended to parallel the diffraction vector (Figures 3(c) and (d)). Since there is no precipitation or any other second phase present in this interface region, it is likely that this modulated diffraction contrast is caused by an inhomogeneous distribution of strains that originate at the interface.

IV. MODELING

The modulating diffraction contrast described in Section III–B, which was only present in the Al_2O_3 filament, could arise from at least two possible sources. There could be a localized strain induced in the Al_2O_3 filament due to variations of the bonding or other localized events. The second possibility could be that misfit edge dislocations could exist at the interface. In other words, the diffraction modulations are on a microscopic scale, *i.e.*, <50 nm. The modulations cannot be due to macroscopic TRS resulting from a difference in the CTE between the matrix and the interface.[7,8]

To investigate the possible role of interfacial strain on the modulating diffraction contrast, an FEM analysis was undertaken to simulate various strain conditions originating from the interface. From these results, TEM diffraction contrast images were then calculated and compared to the observed images. Since the exact distribution of the randomly modulated strain is unknown, the goal of the current modeling was to reveal the basic character of these inhomogeneous strains along the interface. Comparison was made between the calculated images and the experimental images to see if the main important features of the experimental images described could be duplicated by a number of simplified models. Figure 4 is a schematic representation of a portion of the

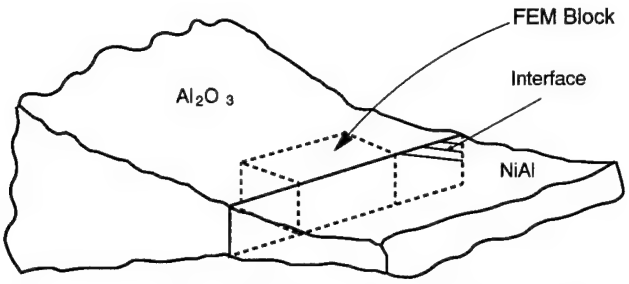

Fig. 4—A schematic representation of a portion of a TEM foil.

TEM foil. The region designated as the FEM block was employed in the modeling. It should be noted that the FEM block is constrained by the large Al_2O_3 filament that is beyond the FEM block. As shown in Figure 5, the inhomogeneity of the strains was simulated as concentrated loads or surface tractions that were applied at the interface in an area.

Several possible loading configurations were examined. First, a concentrated pure shear load was considered, as shown in Figure 5(a). The TRS has been partially relaxed due to TEM sample preparation; *i.e.*, the matrix material has been partially removed from the filament surface, which could cause a shear stress at the remaining interface region. Second, a normal load was considered (Figure 5(b)) since the TRS will also be in the normal direction if it was not completely relaxed. Figure 5(c) presents a case of both shear and normal loading. Surface traction (Figure 5(d)) might also be developed during the sample cooling process, if the bond strength of the interface was not homogeneous.

The FEM elastic analyses employed 3D eight-node linear solid elements and a displacement boundary condition, which gave rise to a maximum strain of ~0.001 at the boundary to produce the observed diffraction contrast level. A maximum strain of 0.001 was used throughout the calculations (the corresponding maximum stress was ~200 MPa in the Al_2O_3). The diameter of the Al_2O_3 filament is so big (125 μm) that the interface can be approximated as a flat plane on a 1-μm scale. According to symmetry, a quarter of the block was considered in all the FEM analyses. An example of the FEM mesh is shown in Figure 6. Because of the nature of thin foils used as TEM samples, the boundary conditions of the FEM block were chosen so that the top and bottom surfaces (plane ABCD in Figure 6) of the block were free of restrictions. Following the symmetry requirement, plane AA′D′D and plane BB′C′C were restricted to move in the *Y* direction and A′B′C′D′ was restricted to move in the *Z* direction. The interface, which was represented by the plane of ABB′A, had no restrictions whenever there was a normal loading at interface as the boundary condition. In the case of pure shear or surface contraction as the boundary condition, the interface was restricted in the *X* direction. The plane CC′D′D was totally restricted in the *X*, *Y*, and *Z* directions due to the fact that very thin regions of the Al_2O_3 filament in the TEM foils were present only in vicinity of the interface; *i.e.*, the foil thickness soon became very thick in the direction toward the center of the filament. Subjected to these boundary conditions, stresses and

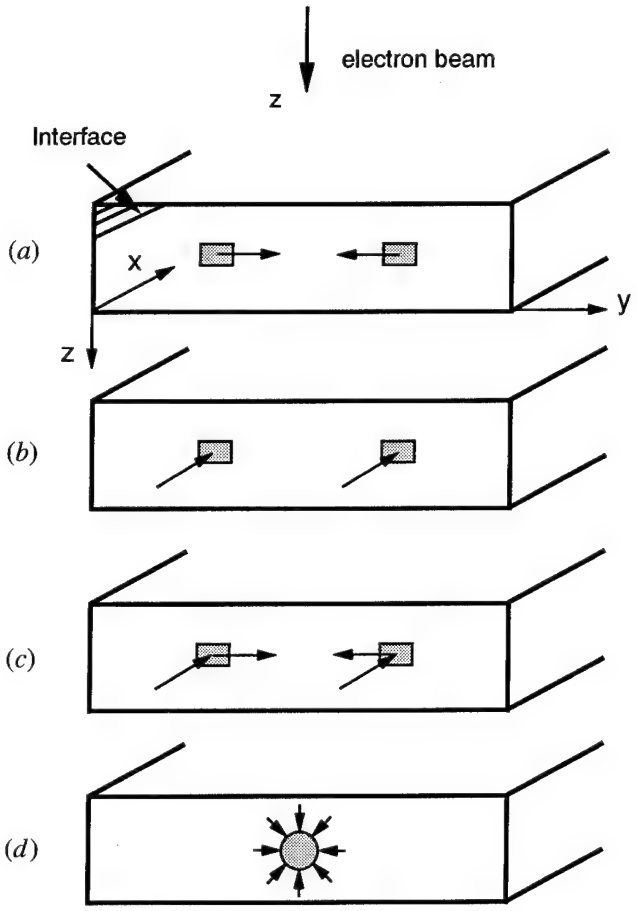

Fig. 5—Schematic illustrations of FEM models of strains introduced at interface: (*a*) concentrated shear load; (*b*) concentrated normal load; (*c*) both the shear and the normal loading; and (*d*) surface traction.

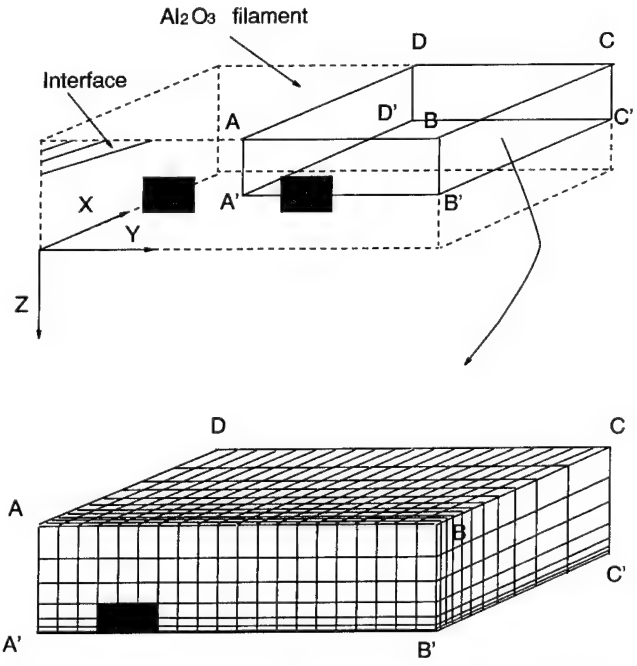

Fig. 6—An example of the FEM mesh where the 3D eight-node linear solid elements were used in all the FEM analyses (see upper figure for boundary conditions).

strains obtained from the FEM analyses were rather localized around the loading area while the top and bottom surfaces were stress free. Stresses and strains near plane CC′D′D and plane BB′C′C were about one to two orders of magnitude smaller than the region close to the loading area.

Simulations of diffraction contrast images are based on the dynamical theory of diffraction contrast in the form developed by Howie and Whelan.[9] When two-beam conditions are applied, the amplitude of the transmitted and diffracted beams, *i.e.*, A_0 and A_g, is determined by

$$\frac{dA_0}{dz} = -\pi a A_0 + \pi(i - a')A_g$$

$$\frac{dA_g}{dz} = -\pi(i - a')A_0 + \pi[-a - 2i(w + \beta')]A_g$$

where

$$\beta' = \frac{d(\mathbf{g} \cdot u)}{dz}$$

In these equations, the depth (z) is normalized by the two-beam extinction distance (ξ_g); $\mathbf{g}$ is the operating diffraction vector; w is a dimensionless form of the deviation parameter; and u is the displacement field within the sample, which causes the diffraction contrast. In the current investigation, u was obtained from the FEM analyses, *i.e.*, the simulated diffraction contrast image was based on the displacement field generated from the FEM analyses. The effect of inelastic scattering was treated phenomenologically by absorption parameters a and a'. Where a is the exponential decay parameter and the a' represents the anomalous absorption. As suggested by Hashimoto *et al.*,[10] and generally adapted by many other investigators, $a = a' = 0.1$ was used in this investigation.

In the calculation of the diffraction contrast image, the whole FEM block was equally divided into 128 × 128 columns parallel to the electron beam direction. The total image size was 128 × 256 columns, which contains twice as many columns as the FEM block (Figure 6). The advantage of using IDL in the programming is that an integration column by column can avoided. The integration can be done in all the columns simultaneously by matrix operation; *i.e.*, each of the variables in the equations can be represented by a 128 × 128 matrix. Integration of the equations started at $A_0 = 1$ and $A_g = 0$. At each integration step, the displacement matrix from the FEM analyses was inserted into these equations. Displacements between the FEM nodes were linearly interpolated from the nearest neighbor nodes. The integration was terminated at the desired foil thickness. The resulting diffraction contrast matrix was then normalized into a 256 gray-level black and white image. Zero intensity was taken as complete darkness in all the simulated images.

The calculated TEM diffraction contrast images corresponding to the loading conditions depicted in Figure 5 are shown in Figure 7. These images were calculated using the same diffraction conditions and foil thickness

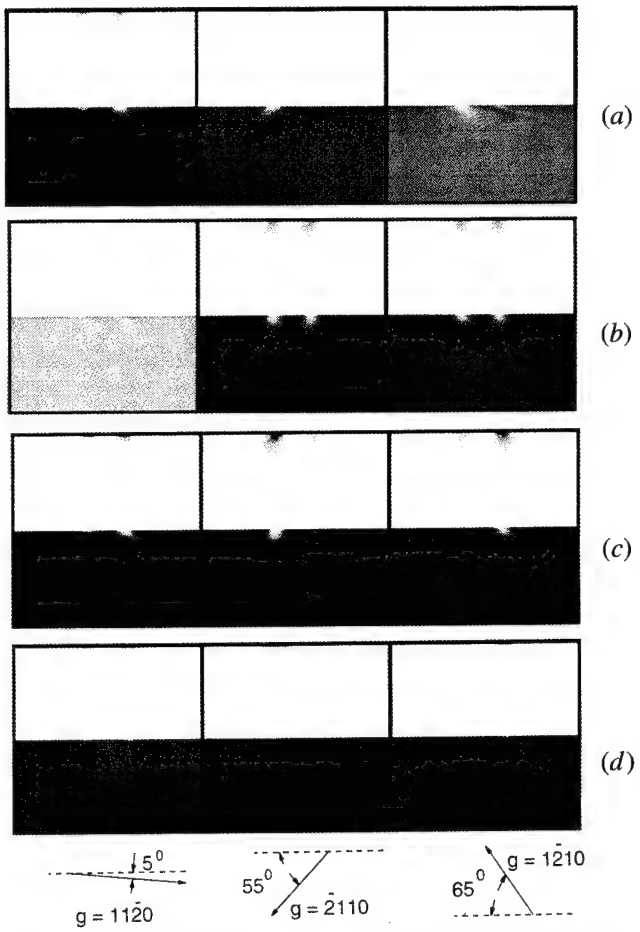

Fig. 7—Bright-field (top) and dark-field (bottom) diffraction contrast image simulations of the FEM model under different diffraction conditions, $w = 1.0$ and $t = 1.3\xi_g$: (*a*) concentrate shear load; (*b*) concentrate normal load; (*c*) both shear and normal; and (*d*) surface traction.

as those of the experimental images (Figure 3). It turns out that only the simple normal loading model (Figure 7(b)) can duplicate all the major features of the experimental images. The contrast is localized around the loading area (in a range of ~0.1 μm from interface), which indicates that the residual strains are concentrated at that region. Furthermore, changes of the location of the loading area in the depth direction (z direction) will not drastically change the basic features of the calculated diffraction contrast images. The size of the area that give the best fit with the observed diffraction contrast corresponds to a region that is 1/4 the thickness of the FEM block. The foil thickness at which the diffraction contrast is observed is ~220 nm; therefore, the size of the loading area is ~55 nm. These size dimensions indicate that we are not dealing with macroscopic (bulk) stress fields, but very microscopic stress fields. Also, changes of the boundary condition, *i.e.*, relaxing the constrain on BB'C'C (Figure 6), to simulate the case that FEM block was near the TEM foil hole, did not change the diffraction contrast pattern.

The possibility of a misfit edge dislocation at the interface of Al_2O_3/NiAl has to be taken into consideration. Figure 8 is a diagram of the position of the edge dislocation at the interface. The edge dislocation angle (α)

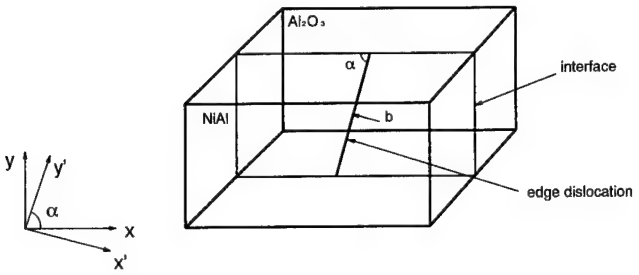

Fig. 8—Schematic illustration of the misfit edge dislocation at the interface between Al_2O_3 and NiAl.

with respect to the electron beam was varied from 90 deg; *i.e.*, the dislocation line was perpendicular to the top and bottom surfaces, to 0 deg, *i.e.*, parallel to the top and bottom surfaces. A FORTRAN program was employed to calculate the displacements in the lattices due to the edge dislocation, and then the contrast images were calculated by use of Eqs. [1] through [3]. The results of these calculations indicated that the contrast from an edge dislocation at the interface was very weak, localized in a region of ~10 nm in size, and the contrast existed on both sides of the interface. This result is in agreement with the previous analysis of Hashimoto and Mannami[11] and Tunstall *et al.*[12]

V. DISCUSSION

A. *Decorated Interface*

After 10 thermal cycles, interfacial debonding of the graphite-decorated interface indicates that the bond strength is poor at such interfaces. The actual separation of the matrix from the filament probably occurred during ion milling of the TEM samples, since the dislocation densities and morphologies in the area adjacent to the debonded interface were identical to that of the bonded interface.[2] The observation of debonding is consistent with previous studies, which concluded that the interfacial bond in P-C processed Al_2O_3/NiAl composites was frictional in nature.[1] With a frictional interfacial bond, whenever the surrounding matrix is partially removed and the filament surface is partially exposed during the ion milling, the TRS will be relaxed and separation of the filament from the matrix will occur.

The graphite formation is suspected to occur during pyrolytic depolymerization of the binders used in the powder cloth method and the high-temperature processing of the composites. The amount of the carbon introduced during the process is far beyond the solubility limit of carbon in the matrix or the filament. The presence of the graphite decoration at the interface apparently weakens the interfacial bond strength of the composite. It is probable that thermal cycling of the composite leads to deformation of the graphite phase resulting in fiber matrix debonding at the graphite phase and a substantial drop in the interfacial bond strength.

B. *Nondecorated Interface*

The modulated diffraction contrast in the Al_2O_3 on the clean interface can be explained by an inhomogeneous distribution of normal stresses along the interface. The data obtained from the simulation indicates that the magnitude of the strain at interface should be at least $\sim 10^{-3}$ and localized around the interface in a range of ~ 0.1 μm. It is unknown why the normal residual strain would modulate along the interface and how it is exactly distributed. One possible reason is that, due to the relaxation of TRS, the plastic deformation in NiAl is not microscopically homogeneous; *i.e.*, the dislocation generation in NiAl created an inhomogeneous "back stress" toward the filament. Since the filament cannot be plastically deformed, this back stress will build up a considerable elastic strain in the filament. One supporting observation is that the modulated diffraction contrast does disappear in a very thin area (less than ~90 nm), *i.e.*, the edge of perforation hole of the TEM foil, where dislocations have escaped from the foil in that area. The disappearance of the diffraction contrast cannot be due to a relaxation of the bounding condition, because the relaxation of the bounding condition does not change the diffraction contrast pattern.

The presence of misfit edge dislocation cannot account for modulated diffraction contrast: the contrast generated by an edge dislocation at the interface is too weak, and exists on both sides of the interface.

Semicoherent interfaces between Al_2O_3 and NiAl have been observed in an XD*-processed TiB_2/NiAl composite that contained Al_2O_3 particles. In that system, low-indexed crystallographic planes of both α-Al_2O_3 and NiAl are aligned.[13] The current investigation does not rule out the possibility of the existence of a semicoherent interface between the Al_2O_3 and NiAl, but none is observed. One important difference between the XD-processed TiB_2/NiAl composite and the current composite is that in the current composite, dislocation generation due to TRS has occurred. This dislocation generation has not been observed in the XD-processed TiB_2/NiAl composite. In general, plastic deformation by dislocation motion is considered microscopically inhomogeneous, and therefore, modulation of strains is expected to occur in all regions of the ceramic-metal interface, where the metal phase undergoes plastic deformation and the ceramic phase remains elastic.

*XD is a trademark of the Martin Marietta Corporation, Bethesda, MD.

VI. CONCLUSIONS

From the data generated in the present investigation, the following conclusions can be drawn.

1. A graphite phase was frequently observed at interfaces in both the as-processed and the thermally cycled composites. The graphite phase formed preferentially at the interface and generally in an island shape. In the as-processed sample, the graphite phase was in intimate contact with both the matrix and Al_2O_3 filament. After 10 thermal cycles, however, the graphite-decorated interface was usually debonded, and deformation of the graphite phase was

evident. The presence at this graphite phase is believed to play a role in the low bond strength in these composites.

2. In regions where the graphite phase was absent, the matrix and filament bonded without any noticeable intermediate layer or precipitates. It is likely that a random direct bond between Al_2O_3 filaments and NiAl matrix was achieved at an atomic level at the clean interfaces. Modulating diffraction contrast along the interface suggests that radial residual strains within the Al_2O_3 are inhomogeneously distributed along the interface. It is believed that the random modulation of the radial residual strains in the Al_2O_3 filament along the interface is caused by plastic deformation of the NiAl matrix.

ACKNOWLEDGMENT

The authors wish to acknowledge the support of NASA Lewis Research Center and the Office of Naval Research under the leadership of Dr. S. Fishman, under Grant No. N00014-94-10118.

REFERENCES

1. R.R. Bowman: in *Intermetallic Matrix Composite II, Materials Research Society Symposium Proceedings*, D.B. Miracle, D.L. Anton, and J.A. Graves, eds., Materials Research Society, Pittsburgh, PA, 1992, vol. 273, pp. 145-55.
2. L. Wang, R.R. Bowman, and R.J. Arsenault: to be published.
3. J.W. Pickens, R.D. Noebe, G.K. Watson, P.K. Brindley, and S.L. Draper: NASA Technical Memorandum 102060, 1989.
4. R.J. Arsenault, L. Wang, and C.R. Feng: *Acta Metall. Mater.*, 1991, vol. 39, pp. 47-57.
5. S.M. Allen: *Phil. Mag.*, 1981, vol. A43, pp. 325-35.
6. P.M. Kelly, A. Jostsons, R.G. Blake, and J.G. Napier: *Phys. Status Solidi*, 1975, vol. A31, pp. 771-80.
7. Q. Ma and D.R. Clarke: *Acta Metall. Mater.*, 1993, vol. 41, pp. 1817-23.
8. J.M. Galbraith, M.N. Kallas, D.A. Koss, and J.R. Hellmann: *Intermetallic Matrix Composite II* Materials Research Society, Pittsburgh, PA, 1992, vol. 273, pp. 119-26.
9. A. Howie and M.J. Whelan: *Proc. R. Soc.*, 1962, vol. A263, pp. 217-37.
10. H. Hashimoto, A. Howie, and M.J. Whelan: *Phil. Mag.*, 1960, vol. 5, pp. 967-74.
11. H. Hashimoto and M. Mannami: *Acta Crystallogr.*, 1960, vol. 13, pp. 363-64.
12. W.J. Tunstall, P.B. Hirsch, and J. Steeds: *Phil. Mag.*, 1964, vol. 9, pp. 99-119.
13. L. Wang and R.J. Arsenault: *Metall. Trans. A*, 1991, vol. 22A, pp. 3013-18.

ELSEVIER

Materials Science and Engineering A201 (1995) 13–23

MATERIALS SCIENCE & ENGINEERING A

Microstructural changes during creep of an SiC/Al_2O_3 composite

J.C. Romero[a], R.J. Arsenault[a], R.F. Krause, Jr.[b]

[a]*Metallurgical Materials Laboratory, Department of Materials and Nuclear Engineering, University of Maryland, College Park, MD 20742-2115, USA*

[b]*National Institute of Standards and Technology, Ceramics Division, Gaithersburg, MD 20899, USA*

Received 13 April 1994; in revised form 2 December 1994

Abstract

The creep properties of an SiC/Al_2O_3 composite were studied under constant-load, four-point flexure tests. The initial stresses ranged from 50 to 350 MPa at temperatures in the range 1000–1300 °C in an air atmosphere. The final strain was as high as 3% at the highest test temperature. A subsequent transmission electron microscopy (TEM) investigation revealed no dislocation generation in the matrix; the few dislocations present were no different than those in the as-made samples. A certain amount of cavitation was observed on the tension face of the specimens tested at 1300 °C. The cavitation was seen to be generated at triple junctions in the matrix and along the whisker/matrix interface. Such cavities then grew into the cracks and, under load, propagated in a mixed mode across the sample. Unaccommodated grain boundary sliding was seen to generate voids along the grain boundaries which then joined into a microcrack and lowered the load-bearing capacity of the composite; this caused a marked drop in the strain to failure of the composite compared with the unreinforced matrix.

Keywords: Microstructure; Creep; Cavitation; SiC/Al_2O_3 composite

1. Introduction

A large variety of structural materials that can be used in a wide range of different engineering applications are required. These materials must be able to withstand high temperatures in very demanding environments where thermal shock and chemical reactivity can deteriorate the mechanical properties. Ceramic materials have the potential to be widely used in these demanding environments due to their very high strength and much stronger resistance to oxidation than most metals. The slow progress in the use of ceramics has been due to two challenging drawbacks; their inherent brittleness and their susceptibility to thermal shock [1]. Therefore it is important to bring about a substantial improvement in the mechanical properties of these ceramics. A method by which this can be accomplished is through the use of composite strengthening, since the use of a ceramic matrix composite can overcome some of the inherent brittleness [2]. It is essential to consider the creep performance of these composites, since excessive deformation at high temperatures will lead to significant degradation of the mechanical properties.

The mechanical performance of these composites is dependent on the individual properties of each of the constituents, the distribution and morphology of the phases present and the properties of the interfaces between the phases. Ceramic composites have not only improved the strength and fracture toughness characteristics of the unreinforced matrix [3–5], but also exhibit a lower coefficient of thermal expansion [6,7] and increasing crack growth resistance [8,9]. However, in order to be used as structural materials, a better knowledge must be acquired of their creep deformation, creep fracture (slow crack growth at high temperatures), thermal shock response and environmental degradation. As it is, ceramic composites show great promise as potential materials for use in heat engines, valve and pump components, extrusion dies, as cutting tools and in diverse applications where cyclic loads are in effect, particularly in compression, since most materials are stronger in compression than in tension.

The present investigation was carried out to examine the creep properties of a 29 vol.% SiC whisker/Al_2O_3 reinforced composite. A number of samples were examined to determine whether any structural changes oc-

SSDI 0921-5093(94)09746-1

curred during testing; these samples were taken from different regions along the creep curve. The purpose was to determine whether there was a change in the creep mechanism between the high and low stress regions (i.e. at high and low strain rates) and, more specifically, to determine whether dislocations played a role in the deformation or whether cavitation or diffusion creep were the dominant mechanisms.

2. Experimental procedure

The mechanical properties and subsequent creep behavior of the composites are dependent on the fabrication methods. In this investigation, the composite was produced by Advanced Composite Materials, Corp. (ACMC), SC. The particulars of the processing are as follows (as supplied by J.F. Rhodes of ACMC). A fine Al_2O_3 matrix powder (1–2 μm) was mixed with SiC whiskers ranging in size from 0.4 to 0.6 μm in diameter and about 5 to 80 μm in length. No additives were added. This mixture (containing 29 vol.% β-SiC whiskers) was then compressed under a uniaxial pressure of 25 MPa at a temperature in the range 1700–1850 °C for approximately 30 min. The density obtained under these conditions is about 95%–99% of the theoretical density [3–5], and the matrix grain size is in the range 1–2 μm, although there are a few grains as large as 8 μm. This procedure leaves the composite with a processing texture, i.e. most whiskers are aligned perpendicular to the hot pressing direction. The flexure specimens used in this investigation were machined so that their prospective tensile faces were normal to the hot pressing direction (this means that the plane containing the long axis of the whiskers is parallel to the tensile surface of the flexure bars).

A four-point flexure test of this composite was carried out in air at temperatures in the range 1000–1300 °C and initial stresses of 50–350 MPa [10]. Beam specimens (3 mm × 4 mm × 50 mm) were prepared and diamond polished to within a 0.01 mm variation in thickness. The testing was done under fixed loads and load point displacements were measured. The load direction was the same as the hot pressing direction. Heating of the specimens, up to the testing temperature, took about 1 h and the samples were held at this temperature for another hour to allow the temperature to become constant across the specimens. Once the testing started, the creep deformation was obtained from load displacements as a function of time, until fracture occurred or until the test was suspended. The displacements were measured by three linear differential transducers. Any displacement fluctuations present in the testing apparatus, due to differential thermal expansion of the apparatus itself or any possible elastic strain produced by the application of the initial load, were subtracted from the displacement measured on the specimen. After the testing had been completed, the furnace was shut off, but the samples were not removed immediately; indeed, some of the samples were left in the furnace for a number of hours before being removed. More details of the testing procedure are given elsewhere [11].

The fracture surfaces and microstructure of the samples before and after testing were investigated by scanning electron microscopy (SEM) and transmission electron microscopy (TEM). To accomplish this, it was necessary to cut a number of slices from each sample. Fig. 1 shows the respective positions of the slices in the bend specimen. One slice was cut perpendicular to the tensile surface which contained the fracture surface itself, while the other slices were cut parallel to the tension face and contained the tension and compression surfaces of the bend beam. This was performed to search for dislocations, cracks and voids in the samples as a function of the distance from the neutral axis and to observe how the cracks propagate across the sample. All slices were polished with a fine grind diamond wheel until a surface suitable for SEM observation was obtained. The SEM investigation was carried out in a JEOL 5400 microscope [1] after the samples had been coated with 30 nm of an Au–Pd conducting film. Some of the samples, those from the high temperature regime, were covered with a thick oxidation layer which formed during testing; these layers had to be ground first in order to expose the underlying microstructure by SEM (there was no grinding of the fracture surface). A number of TEM samples were also prepared from some of the tension and compression slices. The TEM samples were prepared by making a 3 mm disk, using a diamond core drill, from each of the tension and compression slices. These disks were then dimpled, from one side only, using 30 μm diamond paste and a brass wheel, until the thickness at the center of the sample was about 50 μm. Usually, the slices used to prepare TEM samples are dimpled from both sides; in the present case, the slices were dimpled from one side only. The reason for this is that the maximum strain of the sample is obtained at the outer edge of the tension

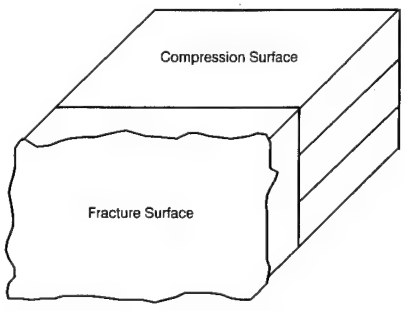

Fig. 1. Location of slices cut for TEM and SEM investigations. The TEM and polished SEM slices were cut perpendicular, while the fracture surface was cut parallel, to the loading axis.

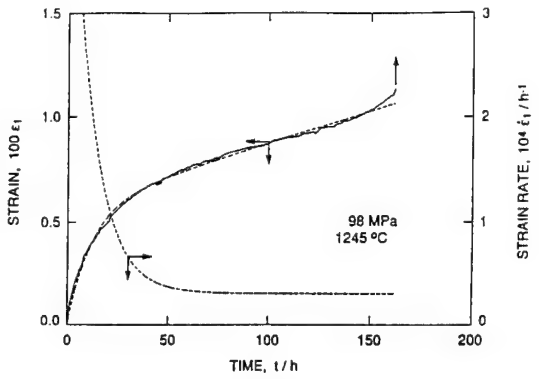

Fig. 2. Primary and secondary creep stages. Although the primary region can be of a substantial magnitude, the secondary region is predominant for at least two- thirds of the testing time. Some samples had to be tested for a long time before steady state was reached.

surface. In order to minimize the loss of material close to the outer edge of the tension surface (due to dimpling), the disk was dimpled only from the side of the disk closer to the neutral axis (i.e. the side further away from the outer edge of the slice containing the tension surface). The samples were then ion milled to perforation using a TECHNICS IV ion mill with an Ar^+ ion beam set at 4 kV and 20° to the sample. Once the perforation was achieved, the orientation of the sample was lowered to 10° and the ion milling operation was continued for another 30 min in order to obtain a larger thinner area more suitable for TEM observation. The TEM studies were performed using the 1 MV transmission electron microscope at the Argonne National Laboratory together with a JEOL 2000 FX-II at the University of Maryland operated at 200 kV[1].

3. Experimental results

The mean strength of the samples, at 25 °C, was found to be 567 ± 11 MPa. This value was constant up to about 800 °C, after which it started to decrease [10]. No measurable creep rates (less than 10^{-7} h^{-1} or 2×10^{-11} s^{-1}) were obtained from flexure tests conducted at 1000 °C over a range of initial stresses from 200 to 374 MPa. The creep curves obtained at higher temperatures exhibited the general typical three stages: primary, secondary and tertiary (Fig. 2 shows a typical curve). However, at low stresses the tertiary stage was not always reached. The creep rate of the composite has, in the past, been found to be as much as two orders of magnitude lower than that of the unreinforced matrix [12,13]. The strain at the outer surface of the beam was evaluated using the method proposed by Hollenberg et al. [14], assuming that the neutral axis is at the center of the beam and that it does not shift during the subsequent deformation.

Fig. 3 shows a plot of the creep strain as a function of time for creep tests at selected stresses at the same temperature. Although primary creep persists for a long period, eventually secondary creep appears to have been attained. It is important to identify the secondary creep mode in order to evaluate a proper value of the strain rate which is invariant with time; otherwise a strain rate ($\dot{\varepsilon}$) taken from the primary mode would be seriously overestimated. This problem is especially likely to arise when creep tests at low bending stresses are prematurely discontinued. Several hundred hours may be required to attain the secondary mode, and thousands of hours may be required before the test ends in failure.

Figs. 4(a) and 4(b) show logarithmic strain vs. stress plots for various temperatures from 1100 to 1300 °C from which the stress exponent (n) can be found. The stress exponent (n) appears in Norton's power law function which is given by $\dot{\varepsilon} = A\sigma^n$, where ε is the strain rate, A is a constant and σ is the applied stress. There are several ways in which to obtain the stress exponent. One approach is to do a least-squares fit of a single straight line through the data at a given temperature. The value of n would then increase from about 5.5 to 17 with increasing temperature from 1100 to 1300 °C, as shown in Fig. 4(a) (note that there is considerable scatter in the data).

An alternative approach is based on an assumption that there is a threshold stress level and that power law "breakdown" occurs at higher strain rates; if this is assumed, then the data can be fitted with three straight lines (Fig. 4(b)). The slope of the full lines, above the threshold point, yields a value of $n = 5.4 \pm 0.4$. The vertical lines on the right-hand side, i.e. higher values of stress at each given temperature, correspond to the

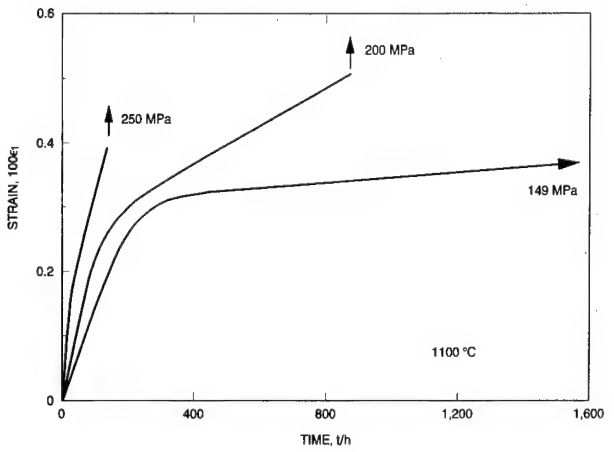

Fig. 3. Selected curves of creep strain as a function of time. These curves are predictions from least-squares fits. The test of longest duration approaches a barely detectable steady state strain rate.

[1] Certain commercial equipment is identified to specify the experimental procedure and does not imply a recommendation by the National Institute of Standards and Technology.

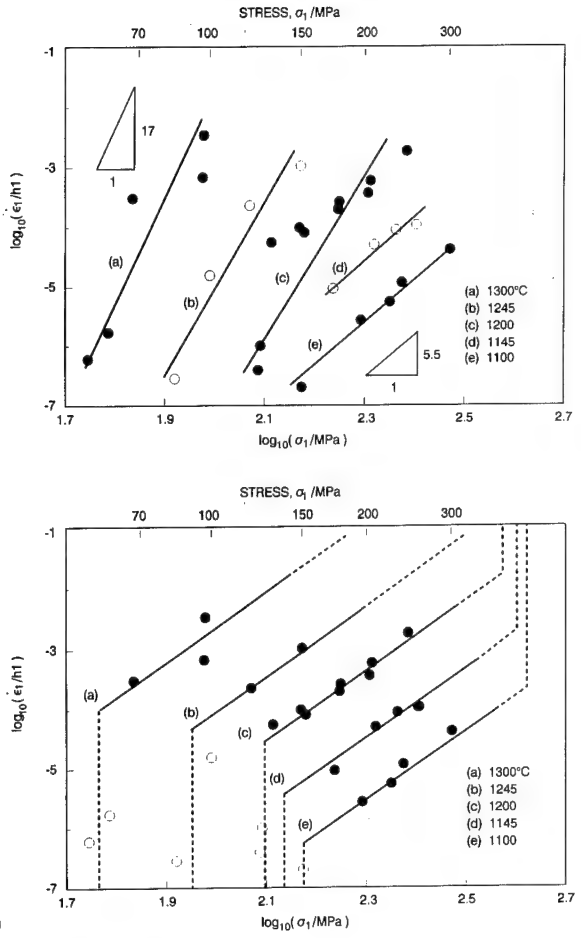

Fig. 4. (a) Logarithmic plots of the steady state strain rate vs. the applied stress, with a least-squares fit through the data points. (b) Logarithmic plots of the steady state strain rate vs. the applied stress. A threshold stress was assumed due to the small strain rates. The vertical line on the right, i.e. higher stress, is the failure load due to rapid loading rates.

stress at which failure occurs due to a rapid loading rate. The broken lines on the left-hand side show regions where $\dot{\varepsilon}$ falls far below that expected by a linear extrapolation from the high stress regime. This may be due to the fact that the steady state strain rates at such low stresses are often barely detectable, i.e. $\dot{\varepsilon} < 10^{-7}$ h^{-1} or 2×10^{-11} s^{-1}; in fact, the low stress samples had to be tested for several hundred hours before exhibiting steady state behavior. Although, in most cases, the steady state was eventually reached and sustained for about two-thirds of the testing time, a considerable primary region was observed in the low stress samples. It was observed that in four-point flexure the low stress tests had to be continued for a very long time before any measurable deformation was detected, while in the high stress tests the samples fractured in a rather short time (less than 1 h in some cases).

The tensile and compressive surfaces of selected samples, from the high and low stress regimes, were first

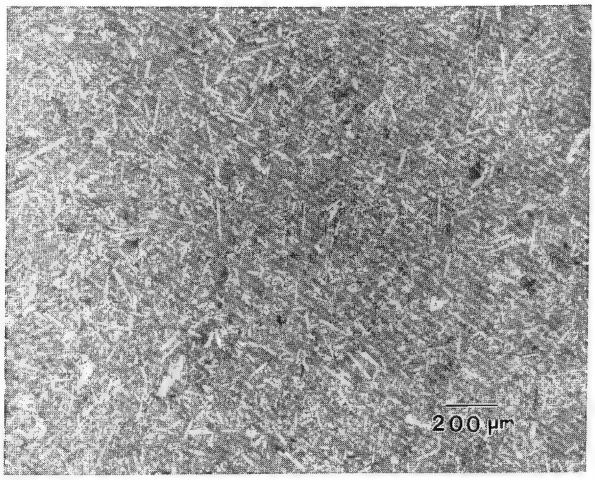

Fig. 5. Optical micrograph showing whisker orientation. Most of the whiskers are seen to have developed an orientation perpendicular to the loading axis, i.e. a planar random array.

metallographically polished with a fine grind diamond wheel and then examined optically. The orientation of the whiskers tends to be, for the most part, perpendicular to the loading axis (i.e. parallel to the tensile surface), as can be seen in Fig. 5, so that there is a planar random array of whiskers. The distribution is not entirely homogeneous; there are a number of very large Al_2O_3 (8 μm) grains, as well as regions that are devoid of any whiskers (these take the shape of rings or river-like forms), as can be seen in Fig. 6.

The subsequent TEM examination revealed no substantial dislocation activity in any of the samples; most of the dislocations observed were confined to large Al_2O_3 grains and the distribution and density of such dislocations did not show any change compared with those samples which were not tested; a typical set of

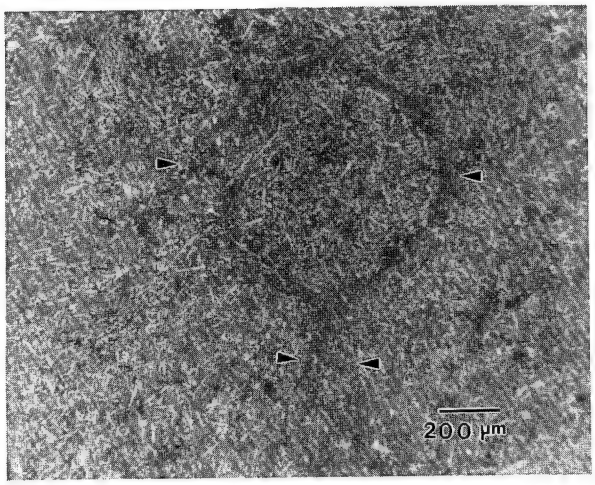

Fig. 6. Inhomogeneities in the whisker distribution. Some regions, as shown by the arrows, are devoid of whiskers and form either rings or thin rivers of unreinforced material. These regions have been observed as the failure initiation points.

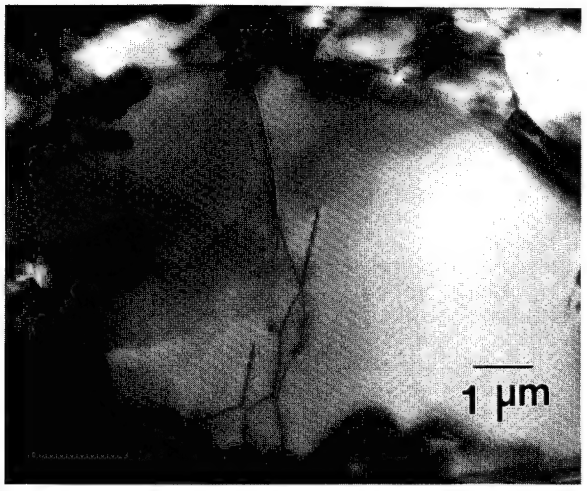

Fig. 7. Typical dislocations in the matrix grains. A similar structure is seen in all samples. Most of the dislocations were seen only in some of the large matrix grains.

dislocations can be seen in Fig. 7. Thus dislocation glide/climb is not expected to play a major role in the deformation of this composite.

Since dislocations were not observed to contribute to the deformation of the composite, the microstructure of the composite was checked more carefully to observe the changes that occurred during deformation. Fig. 8 shows a transmission electron micrograph of the "as-made" sample. Significant cavitation and a high dislocation density were not observed in the sample. Also, TEM examinations at higher magnification did not reveal any amorphous layer at the interface between the SiC whiskers and the matrix. Similar conclusions can be made concerning the samples tested at 1000 and 1100 °C. However, this is not the case for samples tested at 1300 °C; it can be seen from Fig. 9 that a number of cavities are present in the sample. Closer examination

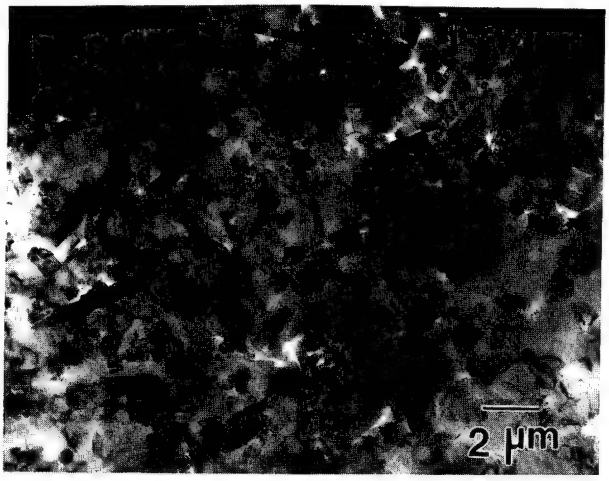

Fig. 9. Tension surface at 1300 °C. High stress regime. Notice the preponderance of voids. Some are the result of cracks and some are due to debonding. Such features were not observed in the "as-made" samples or those tested at lower temperatures. The operating voltage was 1 MV.

showed that the vast majority of these "holes" were produced during the deformation of the sample and were not an artifact of ion milling. Such features were not observed in ion milled foils from samples tested below 1200 °C. All of the TEM observations reported were obtained from foils as close as possible to the tensile surface. Figs. 8 and 9 were taken at an operating voltage of 1 MV, so that a relatively large area could be examined in a given micrograph; these are representative of the numerous foils examined.

Thus it can be said that the generation of voids and microcracks was the major microstructural change observed during the deformation of the composite material tested at 1200–1300 °C at stresses corresponding to the power law region of stress. Fig. 10 shows a higher

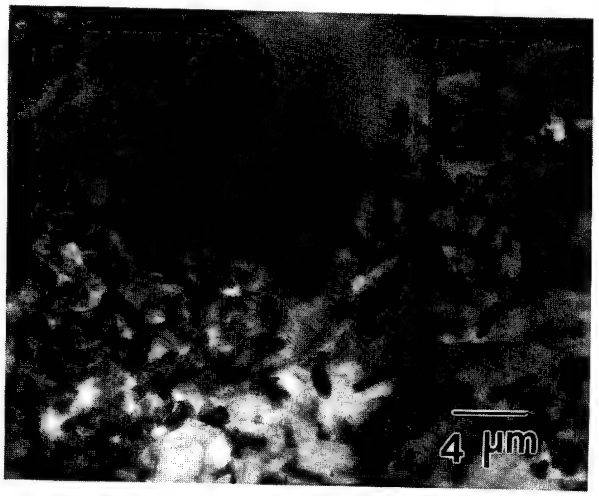

Fig. 8. Transmission electron micrograph of sample in the "as-made" condition. No voids are seen in the sample. The operating voltage was 1 MV.

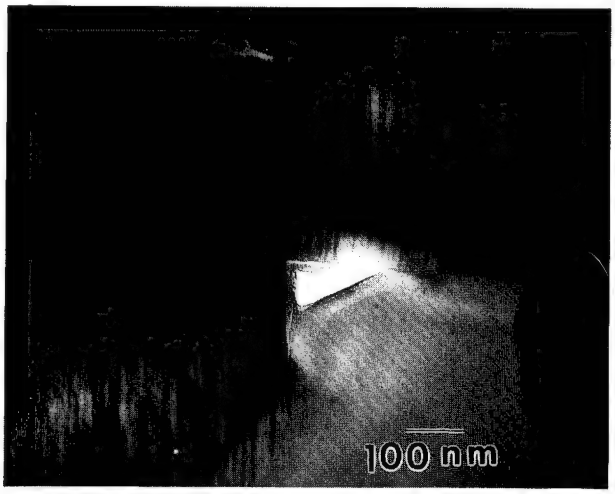

Fig. 10. Cavity formed at whisker/matrix boundary. Such a cavity will, under load, be propagated in an intergranular mode across the matrix.

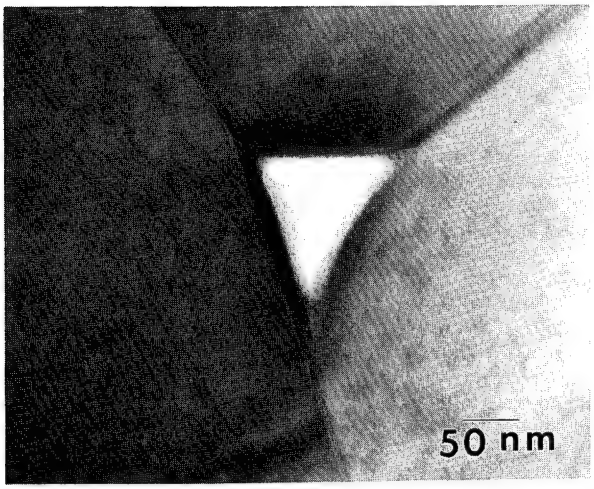

Fig. 11. Cavities formed at triple points in the matrix. These cavities can be the result of grain boundary sliding due to the presence of a glassy phase.

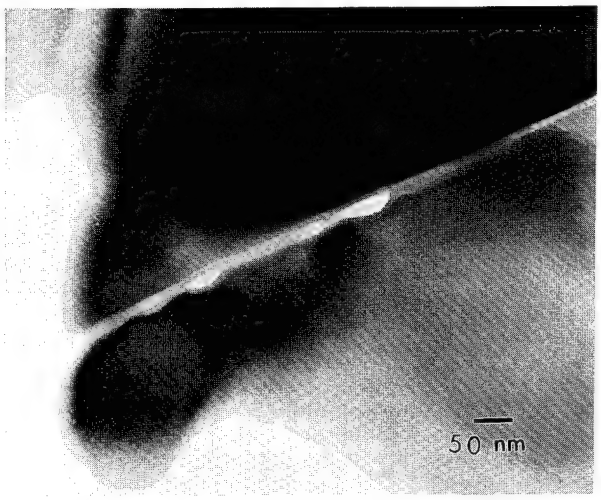

Fig. 13. Formation and coalescence of voids in the matrix. These can grow and join to form an intergranular crack, which can then transform into a mixed mode as the crack interacts with the whiskers.

magnification view of a typical cavity formed along the length of a whisker, while the production of cavities at triple points in the matrix is illustrated in Fig. 11. The formation of these cavities may be due to the accumulation of a glassy phase, either during the fabrication of the composite or due to subsequent oxidation of the whiskers during the deformation of the composite at high temperatures. In this regard, it has been observed that regions of low whisker concentration appear to be devoid of any glassy phase. This glassy or amorphous phase was not observed in the "as-made" composites. Within these regions (see Fig. 12 which can be contrasted with Fig. 11), the triple junctions have a "closed" morphology and there is no evidence of any steps, corrugations or facets along the grain boundaries.

Transmission electron micrographs, as shown in Fig. 13, demonstrate the formation of cavities along the grain boundaries. The rapid growth and coalescence of these cavities ultimately results in the formation of intergranular cracks as observed in Figs. 14 and 15. The crack can then, at first, propagate intergranularly and, as it encounters the whiskers, it changes into a mixed mode of propagation (i.e. intergranular and transgranular), so that, as shown in Fig. 16, large areas are present where a transgranular mode is observed. All of the TEM results reported were from foils cut as close as possible to the tensile surface of the flexure sample. Foils taken from the compression side or the neutral axis location did not exhibit any microstructural changes.

Since the TEM investigation could only reveal information in regions somewhat removed from the fracture surface, SEM investigations were also carried out on the fracture surfaces themselves, although some of these could not be used due to the thick oxide layer formed

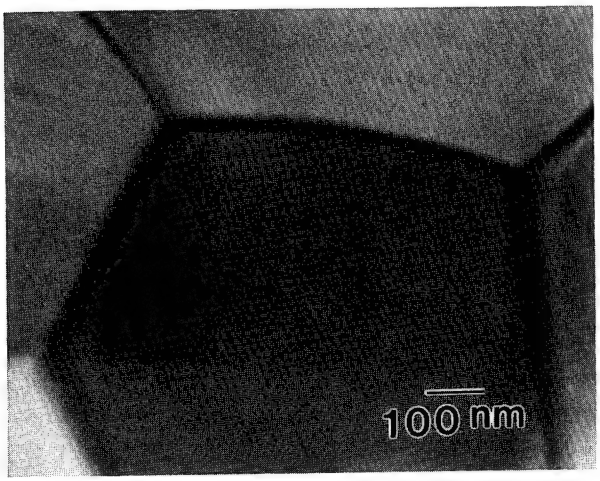

Fig. 12. Continuous boundary among the matrix grains. Grains show no extensive corrugation. This can be indicative of diffusion creep accommodating most of the deformation.

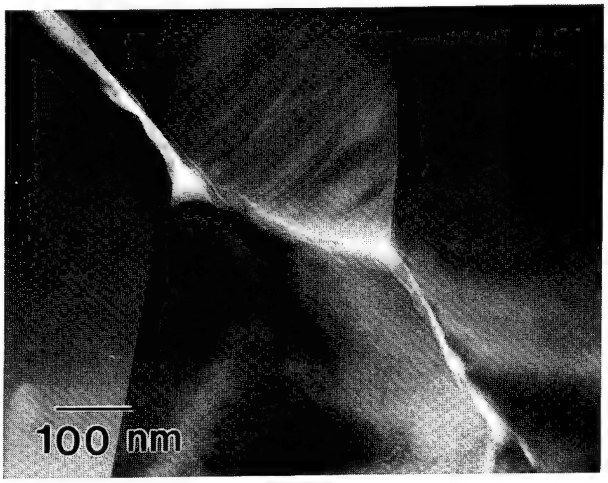

Fig. 14. Formation and coalescence of voids in the matrix.

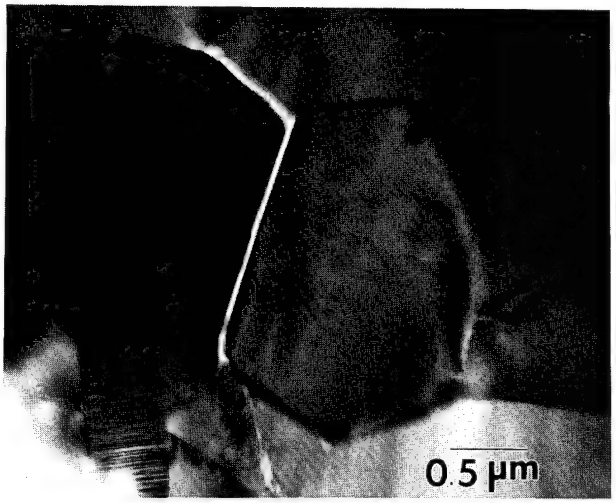

Fig. 15. Propagation of an intergranular crack across the matrix. Such a crack can be the result of the growth of a whisker/matrix cavity, as seen in Fig. 9.

during testing. It should be noted that, as shown in Fig. 1, the central thin area of the TEM samples is located in regions of the sample as far as 2 mm away from the fracture surface. Conceivably, particularly at the lower test temperatures, the deformation may be localized to distances very close to the region of fracture.

A typical fracture surface from the high stress regime at 1100 °C is shown in Fig. 17. The surface shows features of slow crack growth fracture evidenced by the rough nature of the surface topography. Previous research has shown how the SiC whisker/Al_2O_3 system exhibits a substantial crack arrest beyond that of the initial crack growth (i.e. a rising R curve and an increasing value of K_{IC} as the crack length increases) [15,16], which can account for the rough nature of the fracture surface observed in Fig. 17.

Fig. 18 shows a high magnification micrograph of the same surface as in Fig. 17; there is evidence of some

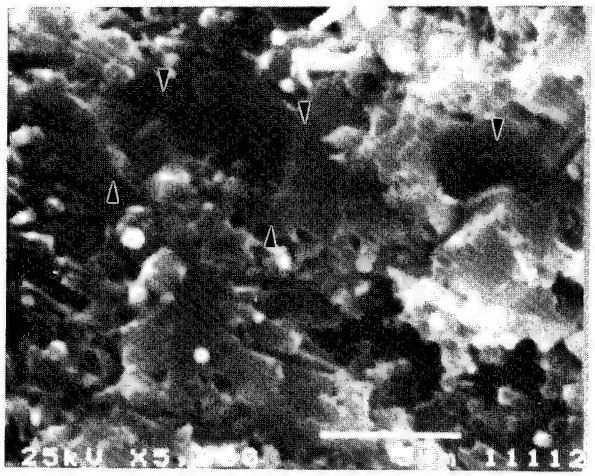

Fig. 16. Transgranular crack propagating across the matrix (see arrows).

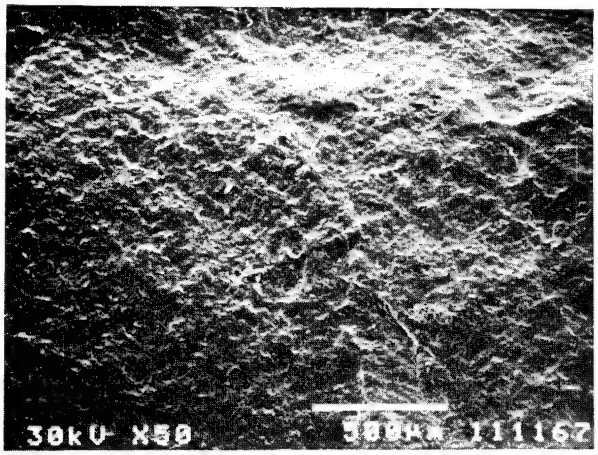

Fig. 17. Rough fracture surface of sample tested at 1100 °C. The rough nature implies a slow crack growth mode, dependent on deformation and not on catastrophic failure.

whisker pull-out, intergranular fracture and some crack deflection around the whiskers. Some voids are also observed on the surface, i.e. the features seen at 1300 °C in TEM are also observed at lower temperatures, but, in this case, the cavities appear to be confined to regions close to the crack propagation path.

The environment to which the composite is exposed is also of great concern, since any significant oxidation of the whiskers that may occur could lead to glass formation at the surface, which will cause creep-generated damage to appear in the form of cracks nucleated even at low temperatures [17,18]. This is so because the glassy phase formed at the surface, or in the cracks generated on the surface, will flow along the grain boundaries and interfaces, which will, in turn, weaken the bond between the matrix and the reinforcement, leading to a reduction in the composite's creep resis-

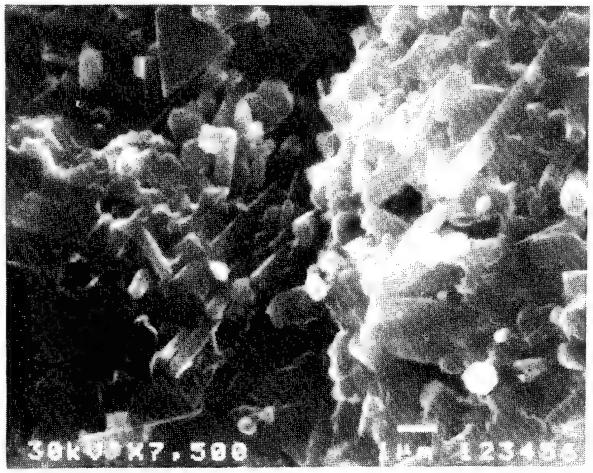

Fig. 18. Fracture surface of sample tested at 1100 °C. As these cracks, formed internally or at the surface flaws, begin to propagate, there is a significant crack deflection around the whiskers which accounts for the increased creep resistance.

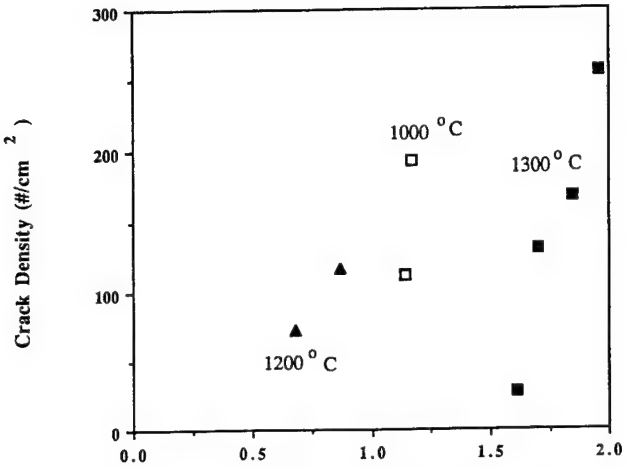

Fig. 19. Crack density as a function of the final strain on the outer edge of the tensile surface.

tance. Indeed, the formation and growth of cracks on the tensile surface were the limiting factors contributing to such a small deformation (i.e. limited to a final strain of less than 3%). The density of surface cracks increased as a function of stress and temperature, being very low at 1100 °C or less and increasing quite rapidly above 1250 °C. The crack density as a function of the final strain on the outer edge of the tensile surface is shown in Fig. 19. The examination of sections cut parallel to the bend axis showed that the cracks formed at temperatures below 1200 °C were confined to a depth of about 300 μm from the tensile surface. On the other hand, at 1300 °C, the cracks were seen to have penetrated to a depth of up to about 600 μm from the tensile surface.

Metallographic observations (see Fig. 6) show the presence of a number of processing flaws, such as very large Al_2O_3 grains (which were present in both the tested and non-tested samples), regions of whisker conglomeration and thin, yet long, whisker-free regions in the matrix. It is these processing flaws which are expected to act as places where the failure of the composite originates in the form of cracks propagating across the tensile surface. The nucleation of cracks was found to be uniform across the tensile surface; there were cracks of various lengths, but the width was rather constant (see Fig. 20). Fig. 20 also shows the unusual case of a very long crack which occurs at high stresses and temperatures.

4. Discussion

From the microstructural results, several observations can be made. Dislocation activity was found to be minimal in this SiC/Al_2O_3 composite; this indicates that a glide- or climb- controlled dislocation mechanism is not operative. There is also no apparent shape change of the grains as a function of temperature or stress. In the temperature range 1200–1300 °C, there is evidence of the generation of voids at grain triple junctions and at the whisker/matrix interface. Also, there is evidence of microcracking; this extends towards the neutral axis, although on the compressed side of the neutral axis there is no evidence of voids or microcracking. Finally, at lower temperatures, such as 1100 °C, although there is no evidence of voids in the TEM foils, there is some evidence of void formation at the fracture surface.

The major macroscopic observation is the presence of cracks on the tension surface of the crept samples. It has been proposed in the past that the generation of surface cracks in a sample can lead to a noticeable strain which, in some cases, might overshadow the actual plastic deformation of the sample itself. The relevance of these models can be seen by comparing the total experimental strain measured with that calculated according to the models proposed by Weertman [19] and Hasselman and Venkateswarn [20], in which a large portion, if not all of the deformation, originates from crack-enhanced and/or elastic creep. Such a relationship (in our case only the Hasselman equation holds, i.e. no dislocations are present in our samples) is shown below

$$\varepsilon = (1 + 2\pi N a^2)\sigma_0/E_0 \quad (1)$$

where ε is the strain, a is the crack half-length, N is the crack density (cm^{-2}), σ_0 is the initial stress (MPa) and E_0 is Young's modulus (GPa).

For large surface crack densities, it might be possible for the crack strain contribution to be a substantial part of the total deformation observed; in such cases, the crack contribution should be subtracted from the total strain. The results for our investigation are summarized

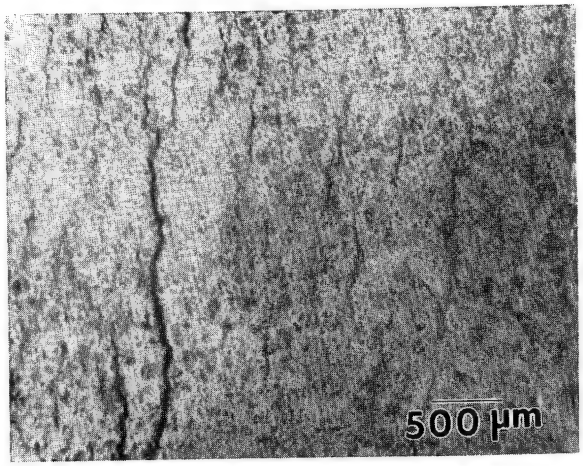

Fig. 20. Distribution of cracks on the tensile surface at 1300 °C. High stress regime. The cracks can be seen to be homogeneously distributed. There is a preponderance of small cracks.

Table 1
Crack strain as a function of crack length

Temperature (°C)	Initial stress (MPa)	N (cm^{-2}) of half crack length (μm)								Total crack strain (%)
		30	60	95	125	190	250	310	635	
1100	240	0	24	3	6	0	3	0	0	0.0815
1200	135	10	12	14	6	4	2	1	0	0.0602
	168	50	16	15	6	1	2	1	0	0.1054
1250	98	35	56	7	11	5	2	0	0	0.0752
	80	75	20	15	10	8	0	0	1	0.0839
1300	125	230	85	40	37	6	2	1	0	0.1422
	150	30	16	8	2	1	0	0	0	0.0344

N, crack density.

in Table 1, where the crack length distribution was divided into eight groups (30, 60, 95, 125, 190, 250, 310 and 635 μm or longer). Although the experimentally obtained final strain at 1100 °C in the present investigation is only of the order of about 0.2%, it can be seen from Table 1 that the generation of surface cracks accounts for only a very small amount of the total deformation observed. This means that, although the premature onset of cracking can lead to failure of the samples at low temperatures without much deformation, the observed strain is still largely dependent on the deformation of the sample; this becomes even more prevalent at temperatures higher than 1200 °C. At temperatures below 1200 °C, the surface crack density is minimal and fracture occurs due to the growth of a single crack, leading to a small failure strain. As the temperature is increased above 1200 °C, the surface crack density increases rapidly, but, at this point, the total deformation strain is also much higher so that the contribution of surface cracks to the total deformation is, once again, negligible. Thus, once again, it is seen that the formation of cracks on the tensile surface cannot account for the non-linearity of the stress exponent during the deformation of the composite material. Further evidence to support this point can be gathered from compression testing of this composite (up to a 10% total strain with no cracking), carried out by Arellano-Lopez et al. [12], which shows the same features as observed here (i.e. no dislocation generation and only a small amount of cavitation). This implies that, although the growth of surface cracks due to any processing flaws in the sample leads to the premature failure of the composite when tested in four-point bend, it is not the cause of the non-linearity in the creep deformation mechanism of the composite.

Finally, this leads us to a consideration of the stress exponent n. If a least-squares plot is made through all the data at a given temperature, n appears to increase from approximately 5.5 to 17 with an increase in the test temperature, but this type of plot indicates considerable scatter in the data. Now, if the threshold stress and power law breakdown are considerable, then in the power law region the stress exponent attains a value of $n = 5.4 \pm 4$. These values of n from 5.4 to 17 indicate that a dislocation mechanism is involved [21]; however, this does not seem to be likely due to the fact that dislocations are not observed, except for those which were initially present.

Lin and Becher [22] found that in 30 vol.% SiC/Al_2O_3, n increased from 3 to 6 with a temperature increase from 1200 to 1300 °C. At 1300 °C and a stress of 100 MPa, the $\dot{\varepsilon}$ values obtained in this investigation and by Lin and Becher [22] are almost the same: 2.8×10^{-7} s^{-1} and 5×10^{-7} s^{-1} respectively. However, at lower stress values, i.e. 60 MPa (at 1300 °C), there is a large difference in $\dot{\varepsilon}$: 3×10^{-10} s^{-1} and 2×10^{-8} s^{-1} respectively. A possible explanation for the difference in $\dot{\varepsilon}$ at the lower values of stress could be related to the definition of the steady state $\dot{\varepsilon}$. In this investigation, steady state $\dot{\varepsilon}$ was only determined after several thousands of hours of creep and at low stresses $\dot{\varepsilon}$ has a tendency to decrease with increasing strain and time.

The most obvious microstructural change is the presence of voids and microcracks, although previous work [23] has shown how the generation of voids and cracks leads to a linear dependence of the strain rate on the stress in the matrix. Since the present value of n is greater than unity, these mechanisms cannot be the cause of the non-linearity of the stress exponent during creep of either the unreinforced matrix or the composite. A similar reasoning rules out grain boundary sliding as the cause of the non-linearity, since the stress dependence is also expected to be linear [24]. Therefore the deformation is a complex form of an interface-controlled mechanism.

In the SiC/Al_2O_3 composite, the whiskers will act as nucleation points for the formation of cavities, which will then grow and coalesce across the sample. This explains the lower cavitation density in the unreinforced Al_2O_3 and also its higher ductility compared with the composite [25,26]. The increased creep resis-

tance observed in this composite can be attributed to significant crack deflection and reduced grain boundary sliding, which are caused by the effect of the SiC whiskers. These whiskers act as an interlocking network of obstacles, which lie across the grain boundaries and retard sliding.

Therefore, on the one hand, the addition of whiskers will present obstacles which a crack impinges upon; it is then deflected and redirected out of the original fracture plane and this tends to lower the deformation rate [27,28]. On the other hand, the presence of whiskers, coupled with the formation and flow of a glassy phase at high temperatures due to whisker oxidation, will promote cavitation and a drop in the load-bearing capacity of the composite, which will result in a lower strain to failure of the composite compared with the single phase Al_2O_3. This correlates quite well with a model proposed in the past, in which, in the early stages of creep deformation, composite strengthening is the result of crack healing, while the latter stages are characterized by a degradation in the mechanical properties due to slow crack growth or creep damage generation [29,30].

Lin and Becher [22] also propose that SiC whiskers enhance the formation of cavitation and that the formation of glassy phases promotes creep deformation by grain boundary sliding. These two effects are the main contributing factors to a value of n of greater than unity. Although the present results lead us to the same conclusion in terms of the deformation mechanism, there is a difference between our n values and those of Lin and Becher [22].

5. Conclusions

The following conclusions can be drawn.

(1) The creep rate of the SiC/Al_2O_3 composite is two orders of magnitude lower than that of the unreinforced Al_2O_3, although the strain to failure is also decreased.

(2) Dislocation glide/climb has a negligible effect on the deformation of the composite.

(3) The formation of voids and microcracks is the most significant microstructural change during creep. Voids, formed at triple junctions or along the grain boundaries, grow and join to yield an intergranular crack; similar microcracks can be seen emanating along the whisker/matrix interface.

(4) Surface cracks form at microstructural inhomogeneities in the sample.

(5) The strain contribution due to surface cracks is less than 0.2% of the total deformation.

(6) The creep mechanism proposed is interface-controlled diffusion creep, accompanied by a small amount of grain boundary sliding, which then leads to the formation of voids and cracks at the interface and along the grain boundaries.

(7) Whisker oxidation, leading to glass formation, reduces the composite's creep resistance by causing interfacial flow to occur at high temperatures.

Acknowledgments

The continued support of Dr. Ed Ryan of the HVEM facility at Argonne National Laboratory is greatly appreciated. This work was partially supported by the Office of Naval Research under grant N00014-94-10118, which is managed by Dr. S. Fishman.

References

[1] W.D. Kingery, *Introduction to Ceramics*, Wiley, New York, 2nd edn., 1976.
[2] T.N. Tiegs and P.F. Becher, *Am. Ceram. Soc. Bull.*, *63* (3) (1984) 463.
[3] G.C. Wei and P.F. Becher, *Am. Ceram. Soc. Bull.*, *64* (2) (1985) 298.
[4] T.N. Tiegs and P.F. Becher, *Am. Ceram. Soc. Bull.*, *66* (2) (1987) 339.
[5] H. Lee and M. Sacks, *J. Am. Ceram. Soc.*, *73* (7) (1990) 1884.
[6] A. Abuhasan, C. Balasingh and P. Predecki, *J. Am. Ceram. Soc.*, *73* (8) (1990) 2474.
[7] S. Majumdar, *J. Am. Ceram. Soc.*, *71* (10) (1989) 858.
[8] M. Jenkins, A.S. Kobayashi, K.W. White and R.C. Bradt, *J. Am. Ceram. Soc.*, *70* (6) (1987) 393.
[9] R.F. Krause, Jr., E.R. Fuller and J.F. Rhodes, *J. Am. Ceram. Soc.*, *73* (3) (1990) 559.
[10] E.R. Fuller, E.P. Butler, R.F. Krause and M.D. Vaudin, *NISTIR-89-4111*, National Institute of Standards and Technology, Gaithersburg, MD, August 1989.
[11] R.F. Krause, Jr. and T.-J. Chang, in P. Vincenzini (ed.), *Ceramics Today—Tomorrow's Ceramics*, Elsevier Science Publishers, 1991, p. 1865.
[12] A.R. de Arellano-Lopez, F.L. Cumbrera, A. Dominguez-Rodriguez, K.C. Goretta and J.L. Routbort, *J. Am. Ceram. Soc.*, *73* (5) (1990) 1297.
[13] J.R. Porter, *Mater. Sci. Eng. A*, *107* (1989) 127.
[14] G.W. Hollenberg, G.R. Terwilliger and R.S. Gordon, *J. Am. Ceram. Soc.*, *54* (4) (1971) 196.
[15] R.K. Govila, *J. Mater. Sci.*, *23* (1988) 3782.
[16] A.A. Morrone, S.R. Nutt and S. Suresh, *J. Mater. Sci.*, *23* (1988) 3206.
[17] S.R. Nutt, P. Lipetzky and P.F. Becher, *Mater. Sci. Eng. A*, *126* (1990) 165.
[18] H. Lin and P.F. Becher, *J. Am. Ceram. Soc.*, *73* (5) (1990) 1378.
[19] J. Weertman, *Trans. Am. Soc. Met.*, *62* (1969) 502.
[20] D.P.H. Hasselman and A. Venkateswarn, *J. Mater. Sci.*, *18* (1983) 161.
[21] K. Xia and T.G. Langdon, in H. Oikawa, K. Maruyama, S. Takeuchi and M. Yamaguchi (eds.), *Strength of Materials*, Japan Institute of Metals, Sendai, Japan, 1994, p. 765.
[22] H.T. Lin and P.F. Becher, *J. Am. Ceram. Soc.*, *74* (1991) 1886.
[23] J.R. Porter, W. Blumenthal and A.G. Evans, *Acta Metall.*, *29* (1981) 1899.
[24] A.H. Heuer, N.J. Tighe and R.W. Cannon, *J. Am. Ceram. Soc.*, *63* (1–2) (1980) 53.

[25] J.R. Porter, F. Lange and A.H. Chokshi, *Am. Ceram. Soc. Bull.*, *66* (2) (1987) 343.
[26] P.F. Becher and T.N. Tiegs, *Adv. Ceram. Mater.*, *3* (2) (1988) 148.
[27] A.G. Evans and W. Blumenthal, in R. Tressler and R.C. Bradt (eds.), *Deformation of Ceramic Materials II*, Plenum, New York, 1983, p. 487.
[28] W. Blumenthal and A.G. Evans, in R. Tressler and R.C. Bradt (eds.), *Deformation of Ceramic Materials II*, Plenum, New York, 1983, p. 555.
[29] H. Riedel, *Fracture at High Temperature*, Springer-Verlag, New York, 1987, pp. 53–62.
[30] S.M. Wiederhorn, in R.C. Bradt, A.G. Evans, D.P.H. Hasselman and F.F. Lange (eds.), *Fracture Mechanics of Ceramics*, Vol. 5, Plenum, New York, 1983, p. 197.

RELAXATION OF THERMAL MISMATCH IN DISCONTINUOUSLY REINFORCED COMPOSITES

N. SHI[1], R. J. ARSENAULT[2], M. A. M. BOURKE[1] AND J. A. GOLDSTONE[1]

[1]LOS ALAMOS NATIONAL LABORATORY

LOS ALAMOS, NM 87545,

[2]DEPARTMENT OF MATERIALS AND NUCLEAR ENGINEERING

UNIVERSITY OF MARYLAND

COLLEGE PARK, MD 20742

Abstract

We have measured the dislocation density and thermal residual elastic strain in NiAl matrices of 20 vol. pct. (V%) Al_2O_3 discontinuously-reinforced composites. As the size of the reinforcement increases the average dislocation density increases, and the corresponding thermal residual elastic strains decrease. The changes with respect to particle size in the dislocation density and residual strain can neither be explained by continuum theory nor by dislocation mechanics for a homogeneous medium. A previously developed model (that satisfactorily describes the SiC/Al system) suggests that the misfit dislocation density decreases with increase in reinforcement size but this disagrees with the current Al_2O_3/NiAl results. A new model is proposed to describe low-symmetry intermetallics, which are constrained in their ability to relax thermal mismatch because of a paucity of independent slip systems. The results are discussed in the context of continuum mechanics using finite element analyses and crystal plasticity.

Introduction

In ceramic reinforced metal matrix composites (MMCs), dislocations are generated during cooling from fabrication temperatures because the coefficients of thermal expansion of the constituents are incompatible [1]. The generation of dislocations has been investigated in several composites such as SiC/Al, Al_2O_3/NiAl and TiB_2/NiAl [1-3].

Several models have been developed to predict the resultant dislocation density, or a continuum equivalent—the average effective plastic strain [4,5]. For example the prismatic punching model developed by Arsenault and Shi [4] predicts that: (1) dislocation density increases with reinforcement volume fraction; and (2) for a constant reinforcement volume fraction, the dislocation density decreases with increasing particle size. These predictions follow because the mismatch prismatic dislocation density is proportional to the total particle surface area. Experimentally the changes in mismatch dislocation density in SiC/Al MMCs follow the prismatic punching model as shown in Fig. 1, $\rho \propto D^{-\alpha}$ [4,6] where D is the particle size.

In polycrystalline low-symmetry intermetallics such as NiAl, slip in individual grains is impeded by a paucity of independent slip systems and the constraint of the neighboring grains. Therefore, the generation of thermal mismatch dislocations is limited by these slip constraints. As in aluminum-based MMCs (where a high dislocation density is beneficial to strengthening), a high density of mobile dislocations in intermetallic composites is desirable for enhancing the ductility. In this investigation, matrix thermal residual elastic strains and matrix dislocation densities were determined in Al_2O_3-reinforced NiAl using neutron diffraction and transmission electron microscopy (TEM), respectively. The effects of different reinforcement sizes and morphologies were examined and compared with SiC/Al MMCs.

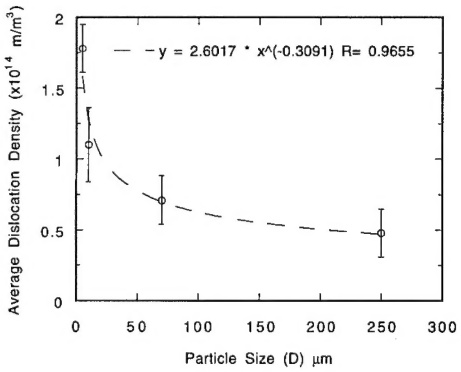

Figure 1 Average matrix dislocation density in annealed 20 V% SiC/Al composite as a function of particle size.

Experimental Procedure

Five 20V% Al_2O_3/NiAl samples were produced with varying reinforcement sizes and shapes; equiaxed particles (hereafter referred to as spheres) with diameters of 5, 75, 355 μm, short fibers and continuous filaments. For the 5 and 75 μm spheres matrix and reinforcement powders of the same size were blended during premixing. For the 355-μm spherical and short-fiber (diameter of 10 μm and average aspect ratio of 10) composites, 75 μm NiAl powder was premixed. The powder mixtures with different particle sizes and morphologies were separately hot pressed at 1623 K for 4 hours at 25 MPa. The continuous filament (diameter of 144 μm) composite was fabricated by a powder cloth technique. All samples were annealed at 1673 K for between 1 and 4 hours followed by furnace cooling. Since a similar powder metallurgical procedure was applied to the fabrication of all specimens (except the filament composite), the as-processed matrix microstructure should be similar in all cases (detailed grain size is not yet available due to a lack of suitable etching solution).

TEM analyses were performed with operating voltages of 200 KV and 1 MV. Sample preparation and data analysis are described elsewhere [7]. Thermal residual elastic strains were measured using the high resolution powder diffractometer at the ISIS facility of the Rutherford Appleton Laboratory, UK. Elastic strains were determined from changes in the lattice constants of the composite matrix (NiAl) with respect to a strain-free reference. Lattice constants (a) were determined by fitting of the complete diffraction patterns that are determined in a time-of-flight measurement using Rietveld refinement [8]. During the refinement a starting diffraction pattern is constructed from the crystal structures of all phases. The

Micromechanics of Advanced Materials:
A Symposium in Honor of Professor James Li's 70th Birthday
Edited by S.N.G. Chu, P.K. Liaw, R.J. Arsenault, K. Sadananda,
K.S. Chan, W.W. Gerberich, C.C. Chau, and T.M. Kung
The Minerals, Metals & Materials Society, 1995

lattice spacing (d_{hkl}) is then least-squares-fitted to the neutron data without alteration of the crystal structures. The results represent the best crystallographic equivalence of an aggregate of homogeneously deforming crystals to the real specimen. More details were described by Bourke et al. [9,10]. FEM modeling was performed using ABAQUS™. Meshes representing two dimensional axisymmetric unit cells containing spherical, short and continuous cylindrical reinforcements were constructed with periodic boundary conditions. A similar procedure is described elsewhere [5,11].

Results

The dislocation densities obtained by TEM for the various shapes and sizes of the Al_2O_3 reinforcement are shown in Figs. 2a and 2b. Although the data are limited, the increase in dislocation density with reinforcement size, as well as between discontinuously reinforced (spheres and short-fibers) and continuous filament is apparent. Comparing Fig. 2b with Fig. 1, the changes in dislocation density as a function of the reinforcement size show opposing trends for the Al_2O_3/NiAl and the SiC/Al. Furthermore, the dislocation density for the 75 μm (spherical particle) composite is higher than that for the short-fiber composite (Fig. 2a), despite the fact that the total matrix/reinforcement interface area for the latter is more than five times larger than that for the former. This contradicts predictions from the prismatic punching model, which predicts an increase in dislocation density with total interface area.

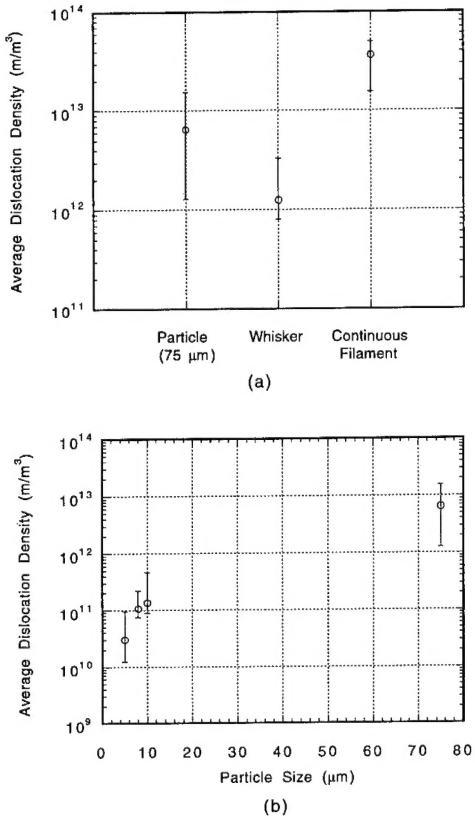

Figure 2 Average matrix dislocation density in annealed 20V% Al_2O_3/NiAl composites as a function of (a) particle shapes, and (b) particle sizes for the spherical composites. The error bar represents the range of data scatter.

Figure 3 shows FEM results relating reinforcement morphology to the average matrix effective plastic strain. Although the effective plastic strain is not expected to vary with the *size* of the reinforcement, it increases as the reinforcement *morphology* progresses from spherical to short-fiber to continuous-filament. Assuming that a fixed portion of the distortion energy is associated with the generation of dislocations (i.e. the dislocation density is proportional to the volume averaged effective plastic strain), the trend of the FEM predictions for the short- and continuous-fiber data (Fig. 3) is consistent with the TEM results (Fig. 2a). However, the continuum (FEM) results in Fig. 3 indicate that the short-fiber composites should be associated with more plasticity than the spherical composite during cooling. As with the prismatic dislocation model, the dislocation densities on the changes from spherical to short-fiber composites (Fig. 2a) disagree with the FEM results.

Table 1 lists the mean phase matrix radial residual elastic strains measured by neutron diffraction in the Al_2O_3/NiAl composites described. During the collection of the neutron diffraction patterns the scattering vectors for all specimens lay in a plane perpendicular to the hot-pressing direction. With planar-isotropism perpendicular to the pressing direction, diffraction results are expected to be independent of any directional anisotropy associated with the pressing procedure. The mean phase residual strains decrease as the particle size increases, but there is a significant increase as the reinforcement morphology changes from equiaxed particles to short fibers. Unfortunately suitable standards were not available for measurement of residual strains in the Al_2O_3. Previous neutron measurements of these composites also show that the radial thermal residual stress for the continuous filament composite is smaller than that of the short-fiber composite (238 MPa for the continuous filament composite [12] and 383 MPa for the short-fiber composite [13]).

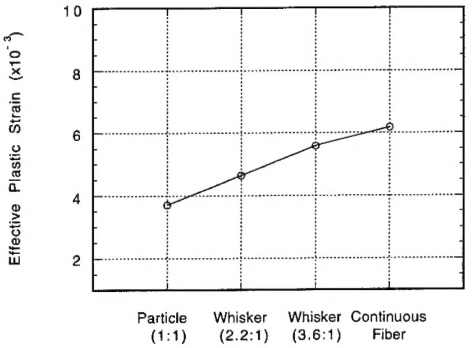

Figure 3 Effective plastic strains predicted by FEM for different reinforcement shapes (particle size does not influence the results).

Table I Matrix Radial Thermal Residual Strain In Al_2O_3/NiAl Composites

Reinforcement (Al_2O_3)Size	Matrix Radial Residual Strains (10^{-4})
5 μm	4.6±0.077
75 μm	3.7±0.098
355 μm	0.87±0.098
Short fiber	8.2±0.098

Comparing the residual strains with the FEM prediction the following trends can be observed: (1) residual strains being dependent on the particle size disagrees with the FEM results; (2) the changes of residual strain from spherical to short-fiber

composites agree with FEM results [2]; and (3) the changes of residual stresses from short- to continuous-fiber composite are inconsistent with the FEM. Although no clear trend can be identified as how the experimental results compare with the models, the dislocation and residual strain data suggest that a single parameter, reinforcement size, dictates the plastic relaxation of thermal mismatch in NiAl composites. The larger the reinforcement size, the more complete the plastic relaxation.

Discussions

Plastic relaxation through dislocation generation requires that thermal mismatch generates stresses that are higher than the matrix critical resolved shear stress (CRSS). Figure 4 shows an FEM prediction of the unrelaxed octahedral shear stress generated by the thermal mismatch, and the uniaxial yield stress for polycrystalline NiAl. The Von Mises yielding criterion is exceeded at all temperatures. This suggests that plastic flow must occur in the NiAl matrix if the principles of phenomenological continuum theories are applicable. The particle-size dependency of the residual strain in the NiAl / Al_2O_3 suggests that although the plastic relaxation does take place, it is very dependent on the microstructural parameters, which cannot be accounted for by continuum theories.

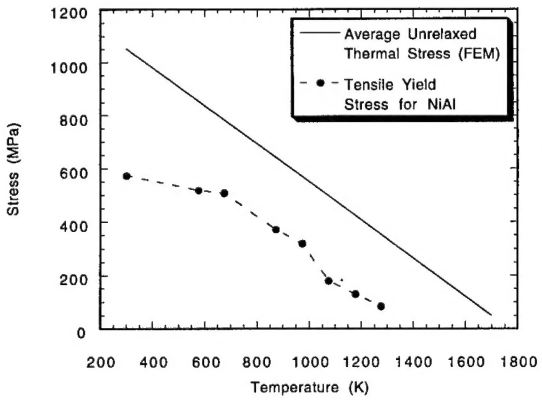

Figure 4 Experimentally measured yield stress of unreinforced polycrystalline NiAl at different temperatures and the predicted matrix thermal mismatch octahedral shear stress without plastic relaxation (elastic matrix).

To understand the difference in SiC/Al and Al_2O_3/NiAl composites with respect to their mismatch dislocation density vs. particle size relationships (Figs. 1 and 2b), one must consider the slip characteristics of the two matrices. Aluminum has an fcc crystal structure with 12 different slip systems of which five are independent. This allows each individual grain to slip independently. In NiAl where the predominant slip system is <100>{100} there are only three independent slip systems [14] with the hard orientation along <100> and the soft orientation along <110> and <111>. The difference in the CRSS between "hard" and the "soft" orientations is about a factor of 14 [15]. According to Von Mises [16], however, self-contained slip within an individual grain of a polycrystalline material requires five independent slip systems without sacrificing intergranular deformation compatibility. Therefore, to avoid creating discontinuities in the NiAl matrix, plastic deformation can occur only when collaborative slip between neighboring grains is activated. This is facilitated when the misfit thermal stress field associated with the reinforcement particles encompasses a greater number of matrix grains, in which case, slip in a particular grain is more likely to be accommodated by flow in other grains.

Figure 5 shows two cases in which the reinforcement size is larger (Fig. 5a) and smaller (Fig. 5b) than the surrounding matrix grains. Due to thermal misfit, a mismatch-affected zone (MAZ) exists around each particle within which a misfit stress develops. The size of the MAZ is proportional, to first order, to the particle size. Thus when the particle size increases relative to the matrix grain size, more matrix grains are encompassed by the MAZ. Then the CRSS is exceeded in many matrix grains and the probability of some having favorable crystallographic orientations for collaborative multi-grain slip increases. Conversely when the reinforcement particle size decreases relative to the matrix grain size, the number of grains in the MAZ reduces and the probability of a favorable grain arrangement for collaborative slip decreases. Thus for a relatively constant matrix grain size plastic relaxation is more likely for large reinforcement particles, supporting the experimental results in this work. Numerical models employing crystal plasticity of polycrystalline aggregates are needed to provide further quantitative understanding of this process.

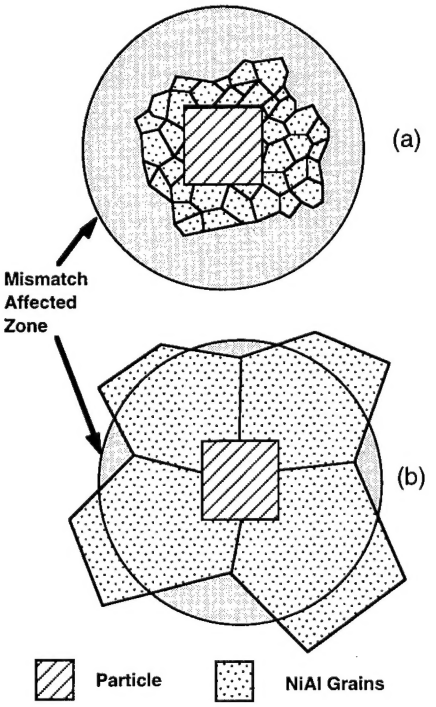

Figure 5 Mismatch affected zone (MAZ) within which large thermal misfit develops. (a) The MAZ is much larger than matrix grains (large particles with constant grain size); (b) the MAZ is much smaller than matrix grains (small particles with constant grain size).

The results reported in Table 1 are derived from changes in the bulk lattice parameters which provide a mean phase average of the residual strain. However this approach of using the Rietveld method hides the anisotropy associated with individual reflections. Single peak fits show that strains along individual directions can vary considerably. For example, in all samples the strains derived from the [100] and [110] reflections are consistently larger and smaller, respectively, than the average from the overall refinement. This indicates more retained thermal mismatch along the hard orientation (less plastic relaxation), and less along the soft orientation (more plastic relaxation). That is, plastic relaxation is grain and orientation sensitive, and is consistent with the deformation mode suggested above. More quantitative analysis of the diffraction data will be reported elsewhere.

The decrease of thermal residual strain with increasing particle size in the Al_2O_3/NiAl composites is also consistent with the deformation modes of multigrain-slip in NiAl. Although continuum

theory predicts an invariance of field quantities to particle size nevertheless the *apparent* polycrystalline yield stress increases with a decreasing particle size when the collaborative slip requirement is impeded in the crystal aggregates. More unrelaxed thermal mismatch is retained in the NiAl with a higher *apparent* polycrystalline yield stress, i.e. a higher thermal residual strain. The residual strain results are also consistent with the TEM dislocation measurements. Therefore, the intergranular-collaborative-slip argument presented herein supports the suggestion that, with relatively constant matrix grain size, the reinforcement size is the single most important parameter that determines the extent of plastic relaxation of thermal mismatch in low-symmetry intermetallic composites.

Conclusions

- In Al_2O_3/NiAl composites the matrix dislocation density from relaxation of thermal mismatch *increases* as the Al_2O_3 particle size increases. In contrast, matrix dislocation density in SiC/Al composite *decreases* as SiC particle size increases.

- The contrast in the dislocation density/particle size relationship for the two composites suggests that plastic relaxation in low symmetry polycrystalline NiAl requires collaborative slip between grains.

- Neutron diffraction results indicate that matrix thermal residual strains in Al_2O_3/NiAl composites decrease as particle size increases, consistent with the variations of dislocation density obtained from TEM.

- The concept of multigrain collaborative slip suggests that the particle size relative to the matrix grain size is the single most important parameter in determine the extent of plastic relaxation of thermal mismatch in low-symmetry intermetallic composites.

Acknowledgment—This work is partially supported by the Office of Naval Research (ONR) under contract N00014-91-J-1353. Support for the neutron diffraction measurements was provided by the US Department of Energy. RJA would like to acknowledge the effective liaison of Dr. S. Fishman of ONR.

Reference

1. R. J. Arsenault, Mater. Sci. Engng., 64 (1984) 171-81.
2. L. Wang, (Ph.D. Dissertation, University of Maryland, 1993).
3. M. Vogelsang, R. J. Arsenault, and R. M. Fisher, Metall. Trans. A., 17 (1986) 379-89.
4. R. J. Arsenault and N. Shi, Mater. Sci. Engng., 81 (1986) 175-87.
5. N. Shi, B. Wilner, and R. J. Arsenault, Acta Metall. Mater., 40 (1992) 2841-54.
6. B. Derby and J. R. Walker, Scripta Metall., 22 (1988) 529-32.
7. L. Wang, R. R. Bowman, R. J. Arsenault, Submitted for publication.
8. R. B. Von Dreele, J. D. Jorgenen, and C. G. Windsor, J. Appl. Crystallogr., 15 (1982) 581-9.
9. M. A. M. Bourke et al., Scripta Metall., 29 (1993) 771-6.
10. M. A. M. Bourke et al., in Proc. of the ICRS IV, (Bethel, CT: Soc. Exp. Mech, 1994), 539-48.
11. N. Shi et al., Metall. Trans. A., 24 (1993) 187-96.
12. A. Saigal and D. S. Kuperman, Scripta Metall., 25 (1991) 2547-52.
13. A. D. Krawitz, private communication with authors, University of Missouri—Columbia, June 1995.
14. G. W. Groves and A. Kelly, Phil. Mag., 8 (1963) 877.
15. R. D. Noebe, R. D. Bowman and M. V. Nathal, Intern. Mater. Rev., 38 (1993) 193-232.
16. R. Von Mises, Z. Angew. Math. Mech., 8 (1928) 161.